

Are you using the right probe molecules for assessing the textural properties of metal–organic frameworks?

Timur Islamoglu,^{1#} Karam B. Idrees,^{1#} Florencia A. Son,¹ Zhijie Chen,¹ Seung-Joon Lee,¹ Peng Li² and Omar K. Farha^{1*}

¹Department of Chemistry and International Institute for Nanotechnology, Northwestern University, 2145 Sheridan Road, Evanston, Illinois 60208, United States

²Shanghai Key Laboratory of Molecular Catalysis and Innovative Materials, Department of Chemistry, Fudan University, 2005 Songhu Road, Shanghai 200438, China

Materials and Methods

All sorption isotherms were collected on a 3Flex (Micromeritics) multiport surface characterization instrument equipped with a turbopump to achieve low pressures required for micropore analysis. MOFs were synthesized and activated according to literature procedures without modification. SmartVapPrep (Micromeritics) was used for temperature-controlled activation of MOF samples under vacuum. BET areas, pore size distributions curves, and pore volumes were calculated using the MicroActive V5.02 (Micromeritics). **Fire Hazard Warning: For oxygen (O_2) isotherms, users must check that the analyzer does not run with a regular oil pump since oxygen can dissolve in oil, which could be a potential fire hazard. Therefore, either an oil free pump or a pump with non-flammable oil must be used for oxygen isotherm measurements.** UHP grade gas tanks for N_2 , Ar, He, Kr and CO_2 isotherms, and UPC grade (99.996%) gas tank for O_2 from Airgas were used for isotherms.

PXRD patterns were collected at room temperature on a STOESTADIMP powder diffractometer equipped with an asymmetric curved Germanium monochromator ($CuK\alpha_1$ radiation, $\lambda = 1.54056 \text{ \AA}$) and one-dimensional silicon strip detector (MYTHEN2 1K from DECTRIS). The generator was set to be 40 kV and 40 mA. Powder was packed in a 3 mm metallic mask and sandwiched between two layers of polyimide tape. The measurement was carried out in transmission geometry in a rotating holder with the intensity data from 1 to 40 degrees. The scan step was set to be $2\theta = 4^\circ$ while the scan time was 60 s per step.

NU-1000, NU-1200, NU-1500-Fe, Mg-MOF-74, UiO-66, ZIF-8, HKUST-1 and MOF-808 were synthesized at Northwestern University, IL, USA. SIFSIX-3-Ni was provided by NuMat Technologies.

Synthesis of NU-1000: A previously published procedure was followed.¹ $ZrOCl_2 \cdot 8H_2O$ (98 mg, 0.30 mmol) and benzoic acid (2 g, 16.38 mmol) were mixed in 8 mL of *N,N*-dimethylformamide (DMF) in an 8-dram vial and ultrasonically dissolved. The clear solution was incubated in an oven at 100 °C for 1 h. After cooling down to room temperature H_4TBAPy (40 mg, 0.06 mmol) and trifluoroacetic acid (TFA) (40 μ L, 0.52 mmol) were added and sonicated for 10 min. The yellow suspension was placed in a preheated oven at 120 °C for 18 h. Yellow polycrystalline material was isolated washed with DMF three times (15 mL each) (soaked ~1 h between washes). An HCl washing step was performed as follows to remove coordinated modulator from the node. The resulting yellow powder was suspended in 12 mL DMF and 0.5 mL of 8 M aqueous HCl was added. This mixture was heated in an oven at 100 °C for 18 h. Isolated powder was washed with DMF three times (15 mL each) and acetone three times (15 mL each) (soaked ~1 h between washes) and soaked in acetone for additional 16 h. NU-1000 crystals were collected by centrifugation and dried in a vacuum oven at 80 °C for 1 h, and then activated under vacuum using Micromeritics Smart VacPrep at 120 °C for 18 h.

Synthesis of NU-1500-Fe: A previously published procedure was followed.² $FeCl_3 \cdot 6H_2O$ (20 mg, 0.074 mmol) and H_6L (10 mg, 0.010 mmol) were dissolved in 3 mL of DMF, and 0.5 mL trifluoroacetic acid (TFA) in a 34 mL Pyrex vial. Then, the mixture was sonicated for 10 min. The resultant mixture was sealed and heated to 150 °C for 12 h. The yellow-orange hexagonal block crystals were obtained. The as-synthesized material was found to be insoluble in H_2O and common organic solvents. Crystals were harvested, washed with DMF for 3 times, and then soaked in DMF overnight. Then the crystals were washed with acetone for 3 times and soaked in acetone for three days followed by activation under vacuum using Micromeritics Smart VacPrep at 130 °C for 18 h.

Synthesis of NU-1200: A previously published procedure was followed.³ $ZrOCl_2 \cdot 8H_2O$ (0.095 mmol, 17 mg), 4,4',4''-(2,4,6-trimethylbenzene-1,3,5-triyl)tribenzoic acid (TMTB) (0.02 mmol, 10 mg), trifluoroacetic acid (150 μ L), and DMF (2 mL) were charged in a 4 mL Pyrex vial. The mixture was heated in a 120 °C oven for 48 h. The solution was removed immediately and the solid residue was washed with fresh DMF three times. Modulator from the node of as synthesized NU-1200 was removed using the same

procedure as for NU-1000 mentioned above but replacing 8M HCl with 4M HCl. The crystals were activated under vacuum using Micromeritics Smart VacPrep at 120 °C for 18 h.

Synthesis of Mg-MOF-74: A previously published procedure was followed.⁴ 0.238 g of Magnesium nitrate hexahydrate, 0.056 g of 2,5-dihydroxyterephthalic acid were dissolved in 22.5 mL of DMF, 1.5 mL of ethanol, and 1.5 mL of water. After sonication, the mixture was decanted into three 4 dram vials and heated in an oven at 125 °C for 21 h. The resulting powder washed with DMF three times and solvent exchanged with methanol for five times, soaking at least 2 h in each solvent replenish. The resulting powder was activated under vacuum using Micromeritics Smart VacPrep at 250 °C for 18 h.

Synthesis of UiO-66: A previously published procedure was followed.⁵ Two separate solutions were prepared by dissolving terephthalic dicarboxylic acid (100 mg, 0.60 mmol) and ZrCl₄ (140 mg, 0.60 mmol) each in 15 mL DMF. The solutions were sonicated for 15 minutes until complete dissolution. The two solutions were then combined and 10 mL AcOH was added before heating the mixture at 120 °C for 3 days. After cooling to room temperature, the sample was centrifuged and washed three times each with DMF and acetone and was allowed to soak in acetone overnight. The sample was dried in a vacuum oven at 80 °C before thermal activation under vacuum using Micromeritics Smart VacPrep at 120 °C for 18 h.

Synthesis of ZIF-8: A previously published procedure was followed.⁶ 350 mg of Zn(NO₃)₂·6H₂O and 200 mg of 2-methylimidazole were placed in a 20 mL screw-top vial and dissolved in 15 mL of DMF. Three drops of HNO₃ were added to a mixture with a Pasteur pipet, and complete dissolution was achieved by sonication. The vial was capped and placed in an oven at 120 °C for 24 h. Crystals were collected and washed with DMF. Solvent exchange was done using methanol followed by thermal activation under vacuum using Micromeritics Smart VacPrep at 120 °C for 18 h.

Synthesis of HKUST-1: A previously published procedure was followed.⁷ In an 8 dram 1,3,5-benzenetricarboxylate (500 mg, 2.38 mmol) and oxalic acid dihydrate (60 mg, 0.48 mmol) were dissolved in 10 mL of EtOH and 1 mL DMF mixture. In a separate vial Cu(NO₃)₂·3H₂O (1.65 g, 6.8 mmol) was dissolved in 9 mL of H₂O and was added to linker solution. The resulting milky suspension was sonicated and placed in 80 °C pre-heated oven for 48 h. The insoluble white precipitate can be easily removed using density separation by adding fresh ethanol and pipetting out the white suspension above the crystals. This can be repeated until the white suspension is completely removed. The resulting blue HKUST-1 crystals were further washed with ethanol and dried under vacuum using Micromeritics Smart VacPrep at 150 °C for 18 h.

Synthesis of MOF-808: A previously published procedure was followed.⁸ ZrOCl₂·8H₂O (160 mg, 0.50 mmol), and 1,3,5 benzene tricarboxylic acid (110 mg, 0.52 mmol) were added in a solvent mixture of 20 ml of DMF and 20 mL formic acid. The mixture was placed in a 100 ml glass bottle and sonicated until the clear solution was obtained. The solution was then placed in a preheated oven at 100 °C overnight. After the material was cooled to room temperature, the product was collected by centrifugation. The product was washed three times with DMF followed by three times acetone washing. The product was left to be soaked in acetone overnight for the complete exchange DMF with acetone in the pores. Finally, the sample was activated under vacuum using Micromeritics Smart VacPrep at 100 °C for 18 h.

Synthesis of SIFSIX-3-Ni: A previously published procedure was followed.⁹ Pyrazine (72.0 g, 0.90 mol) was added to a solution of nickel nitrate hexahydrate Ni(NO₃)₂·6H₂O (130.8 g, 0.45 mol) and ammonium hexafluorosilicate (NH₄)₂SiF₆ (80.0 g, 0.45 mol) in 400 mL water in a 1 L media bottle. The resulting solution was heated in an oven at 90 °C and allowed to solvothermally react for 48 h. The mother liquor was decanted and the crystalline powder was washed with water (1 × 200 mL) for 1 hour. The powder was then washed with hot methanol (7 × 100 mL) over 5 days. The product was dried under vacuum (0.01 Torr) for 24 h at 150 °C. Finally, 58.26 g of product was obtained with a yield of 35.9%. The sample was activated under vacuum using Micromeritics Smart VacPrep at 150 °C for 18 h.

S1: Gas isotherms and pore size distribution plots

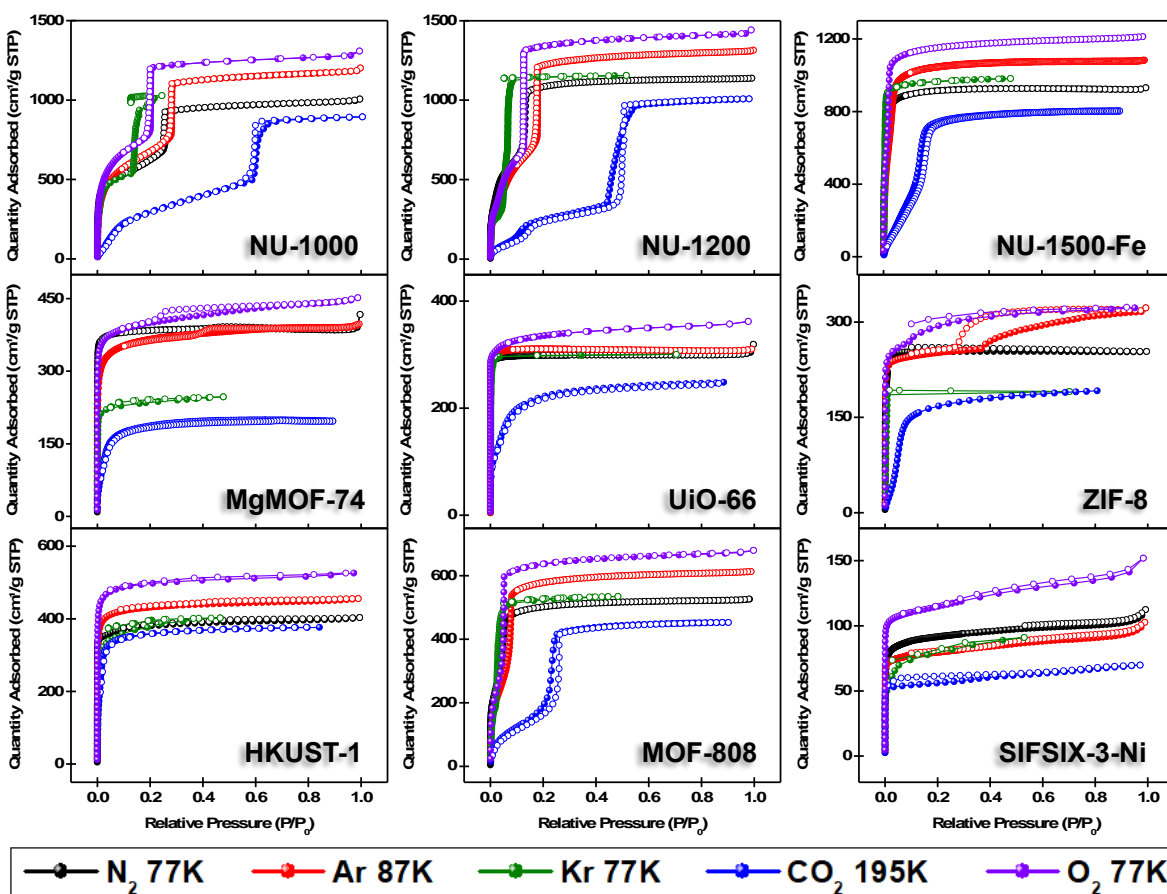


Figure S1. Adsorption (closed symbols) and desorption (open symbols) isotherms of NU-1000, NU-1200, NU-1500-Fe, Mg-MOF-74, UiO-66, ZIF-8, HKUST-1, MOF-808, and SIFSIX-3-Ni using N_2 77K, Ar 87K, Kr 77K, CO_2 195K, and O_2 77K.

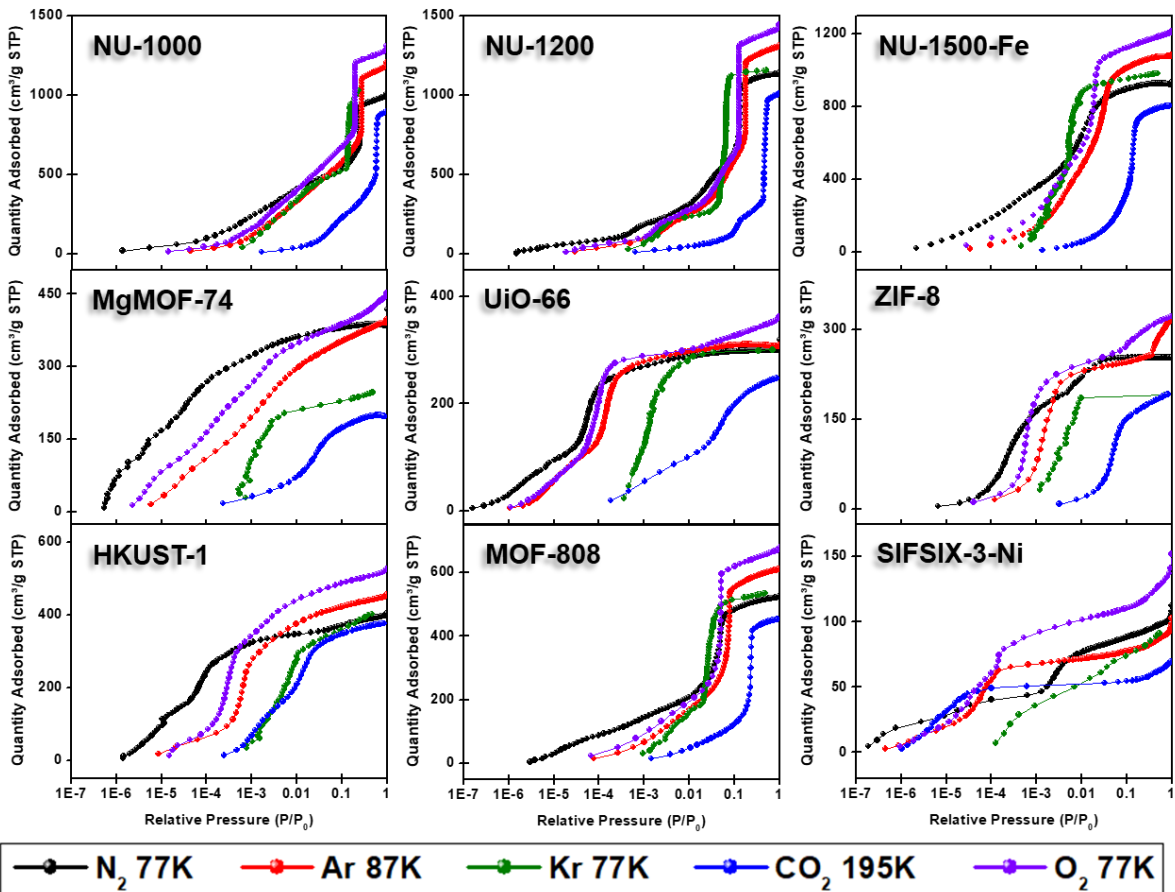


Figure S2. Semi-logarithmic scale adsorption isotherms of NU-1000, NU-1200, NU-1500-Fe, Mg-MOF-74, UiO-66, ZIF-8, HKUST-1, MOF-808, and SIFSIX-3-Ni using N₂ 77K, Ar 87K, Kr 77K, CO₂ 195K, and O₂ 77K.

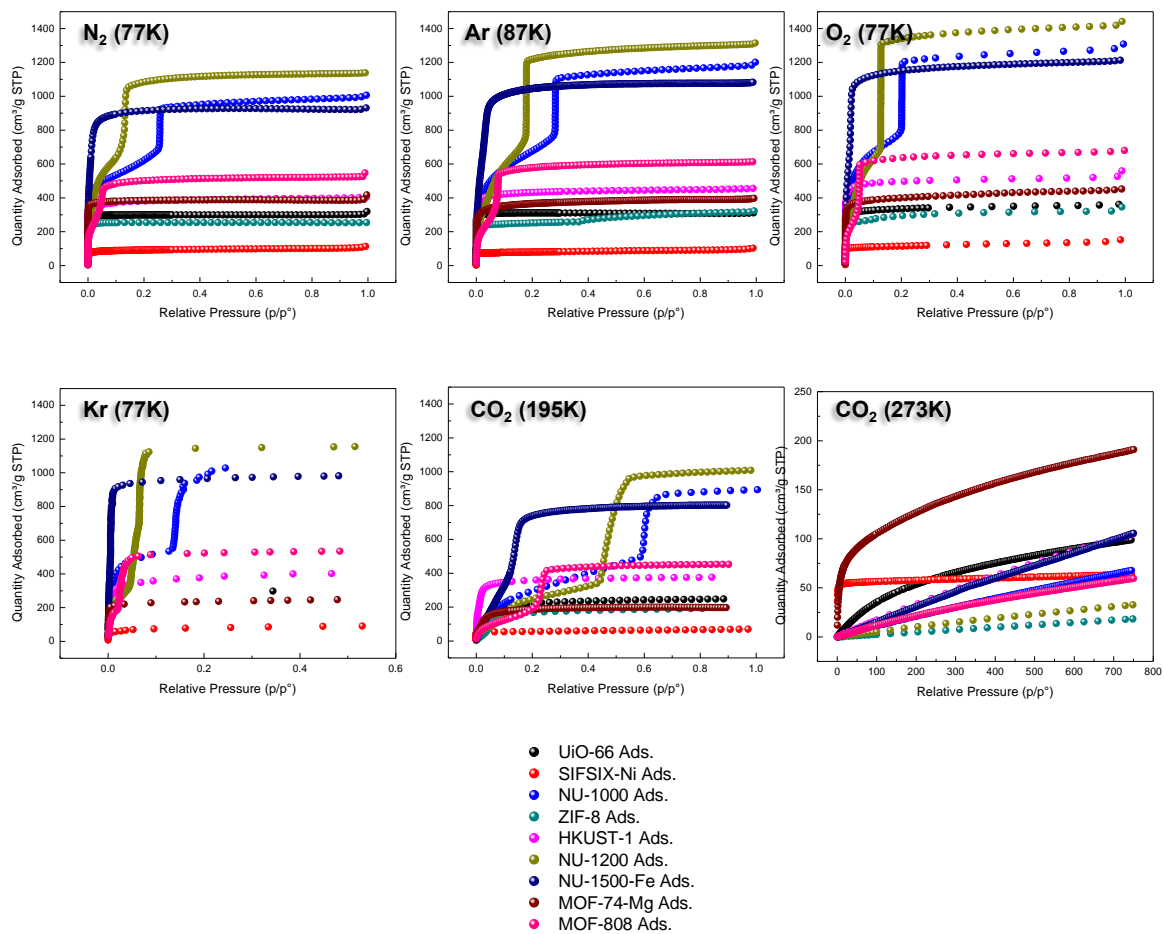


Figure S3. Gas isotherms for NU-1000, NU-1200, NU-1500-Fe, Mg-MOF-74, UiO-66, ZIF-8, HKUST-1, MOF-808, and SIFSIX-3-Ni.

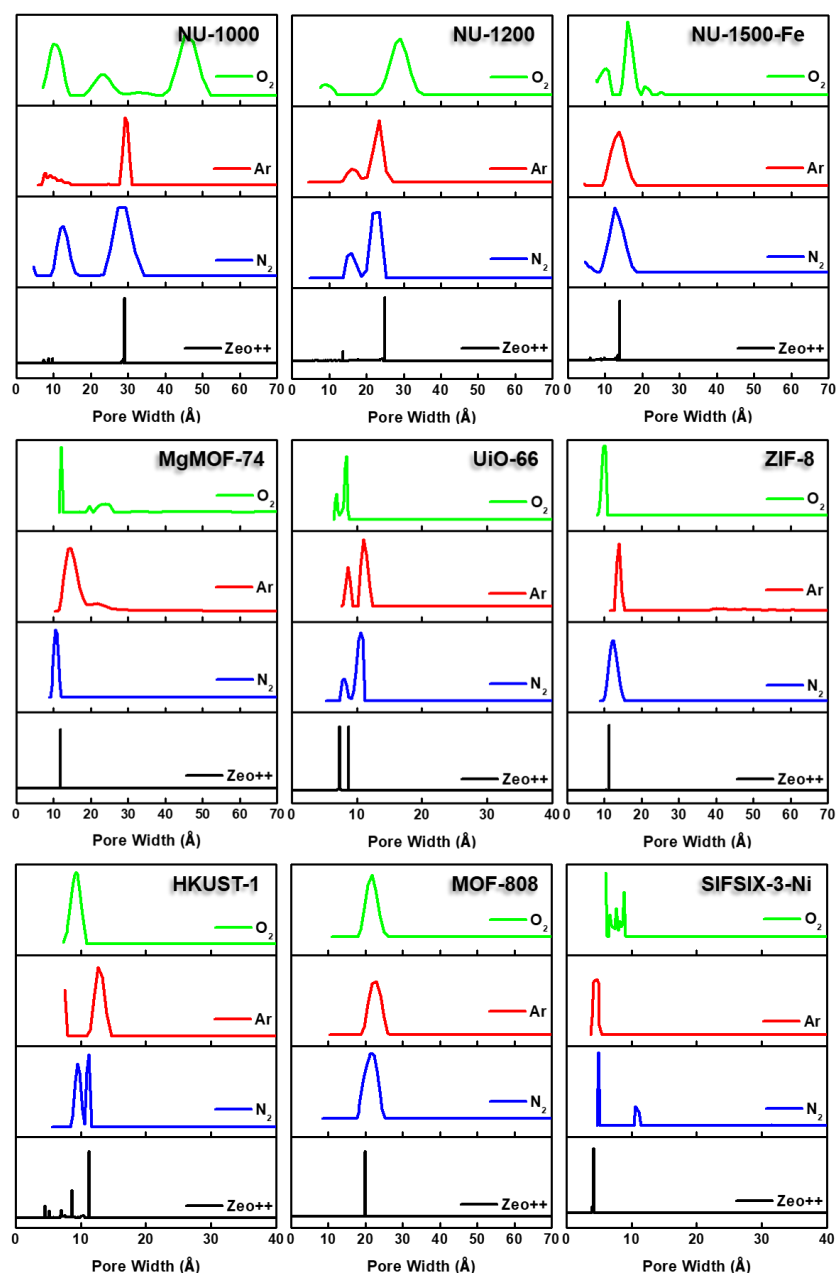


Figure S4. Pore size distribution analysis of NU-1000, NU-1200, NU-1500-Fe, MgMOF-74, UiO-66, ZIF-8, HKUST-1, MOF-808, and SIFSIX-3-Ni using DFT models for N₂ 77K, Ar 87K, and O₂ 77K; and calculated pore size distributions using Zeo++.¹⁰

S2: BET plots and Rouquerol *et al.* consistency criteria

S2.1: BET consistency criteria

1. Only a range where $N(1 - P/P_0)$ increases monotonically with P/P_0 should be selected.
2. The value of C resulting from the linear regression should be positive.
3. The monolayer loading N_m should correspond to a relative pressure P/P_0 falling within the selected linear region.
4. The relative pressure corresponding to the monolayer loading calculated from BET theory ($1/\sqrt{C + 1}$) should be equal to the pressure determined in criterion 3.

Table S1. BET criteria for NU-1000, NU-1200, NU-1500-Fe, Mg-MOF-74, UiO-66, ZIF-8, HKUST-1, MOF-808, and SIFSIX-3-Ni using N_2 77K. T=True (satisfies the criteria); F=False (does not satisfy the criteria).

N_2 77K					
MOF / BET criteria	1	2	3	4	$R^2 > 0.9975$
UiO-66	T	T	T	T	T
SIFSIX-Ni	T	T	T	T	T
NU-1000	T	T	T	T	T
ZIF-8	T	T	T	T	T
HKUST-1	T	T	T	T	T
NU-1200	T	T	T	T	T
NU-1500-Fe	T	T	T	T	T
Mg-MOF-74	T	T	T	T	T
MOF-808	T	T	T	T	T

Table S2. BET criteria for NU-1000, NU-1200, NU-1500-Fe, MgMOF-74, UiO-66, ZIF-8, HKUST-1, MOF-808, and SIFSIX-3-Ni using Ar 87K. T=True (satisfies the criteria); F=False (does not satisfy the criteria).

Ar 87K

MOF / BET criteria	1	2	3	4	$R^2 > 0.9975$
UiO-66	T	T	T	T	T
SIFSIX-Ni	T	T	T	T	T
NU-1000	T	T	T	T	T
ZIF-8	T	T	T	T	T
HKUST-1	T	T	T	T	T
NU-1200	T	T	T	T	T
NU-1500-Fe	T	T	T	T	T
Mg-MOF-74	T	T	T	T	T
MOF-808	T	T	T	T	F

Table S3. BET criteria for NU-1000, NU-1200, NU-1500-Fe, MgMOF-74, UiO-66, ZIF-8, HKUST-1, MOF-808, and SIFSIX-3-Ni using O₂ 77K. T=True (satisfies the criteria); F=False (does not satisfy the criteria).

O₂ 77K

MOF / BET criteria	1	2	3	4	$R^2 > 0.9975$
UiO-66	T	T	T	T	T
SIFSIX-Ni	T	T	T	T	T
NU-1000	T	T	T	T	T
ZIF-8	T	T	T	T	T
HKUST-1	T	T	T	T	T
NU-1200	T	T	F	T	F
NU-1500-Fe	T	T	T	T	T
Mg-MOF-74	T	T	T	T	T
MOF-808	T	T	F	T	F

Table S4. BET criteria for NU-1000, NU-1200, NU-1500-Fe, MgMOF-74, UiO-66, ZIF-8, HKUST-1, MOF-808, and SIFSIX-3-Ni using Kr 77K. T=True (satisfies the criteria); F=False (does not satisfy the criteria).

Kr 77K

MOF / BET criteria	1	2	3	4	$R^2 > 0.9975$
UiO-66	T	T	T	T	T
SIFSIX-Ni	T	T	T	T	T
NU-1000	T	T	T	T	T
ZIF-8	T	T	F	T	F
HKUST-1	T	T	T	T	T
NU-1200	T	T	T	T	T
NU-1500-Fe	T	T	T	T	T
Mg-MOF-74	T	T	T	T	T
MOF-808	T	T	T	T	T

Table S5. BET criteria for NU-1000, NU-1200, NU-1500-Fe, MgMOF-74, UiO-66, ZIF-8, HKUST-1, MOF-808, and SIFSIX-3-Ni using CO₂ 195K. T=True (satisfies the criteria); F=False (does not satisfy the criteria).

CO₂ 195K

MOF / BET criteria	1	2	3	4	$R^2 > 0.9975$
UiO-66	T	T	T	T	T
SIFSIX-Ni	T	T	T	T	T
NU-1000	T	T	T	T	T
ZIF-8	T	T	T	T	T
HKUST-1	T	T	T	T	T
NU-1200	T	T	T	T	T
NU-1500-Fe	T	T	T	T	F
Mg-MOF-74	T	T	T	T	T
MOF-808	T	T	T	T	F

S2.2 UiO-66

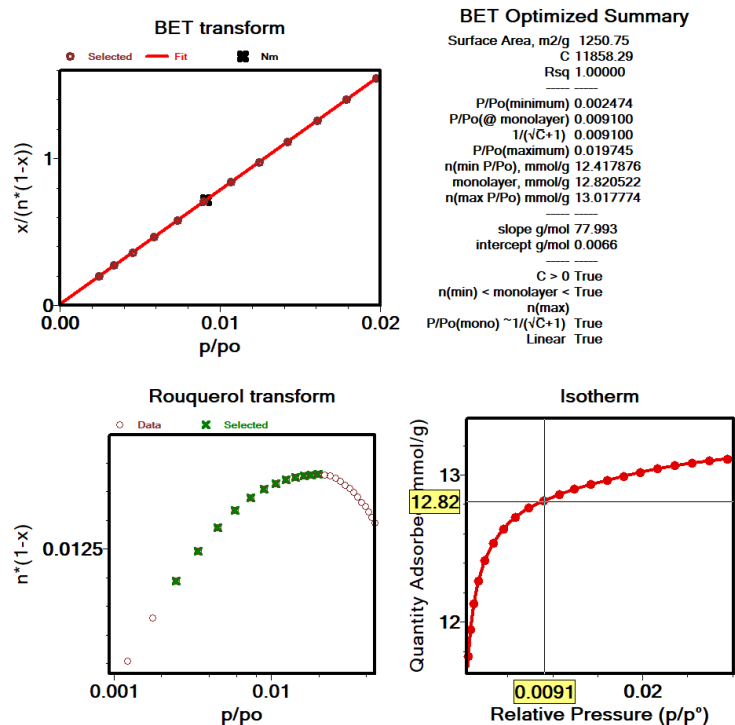


Figure S5. BET transform, Rouquerol transform and BET summary of UiO-66 for N₂ isotherm at 77 K.

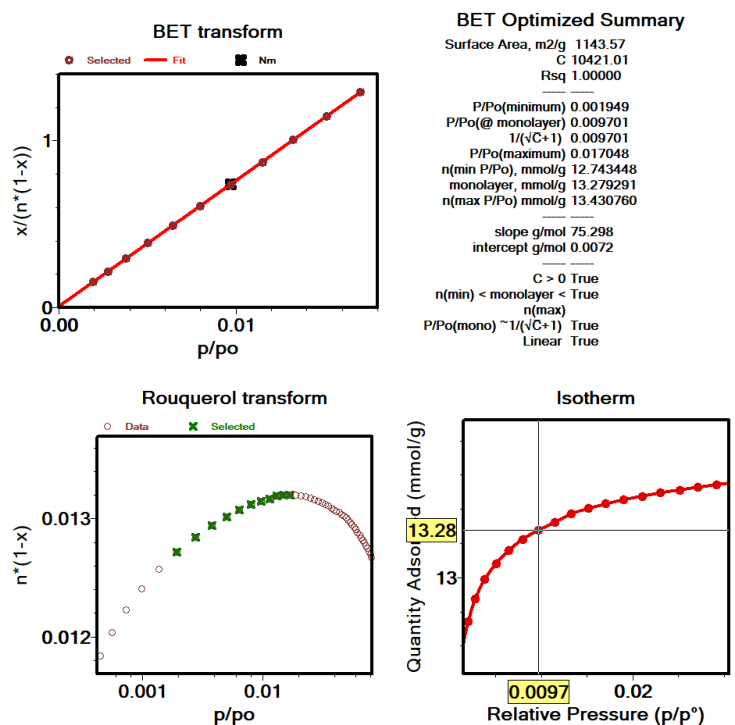


Figure S6. BET transform, Rouquerol transform and BET summary of UiO-66 for Ar isotherm at 87 K.

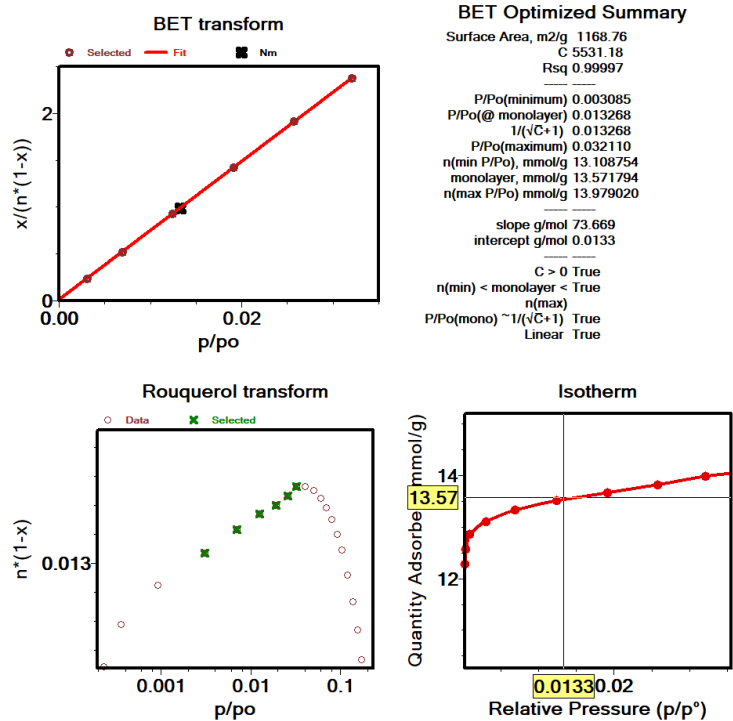


Figure S7. BET transform, Rouquerol transform and BET summary of UiO-66 for O₂ isotherm at 77 K.

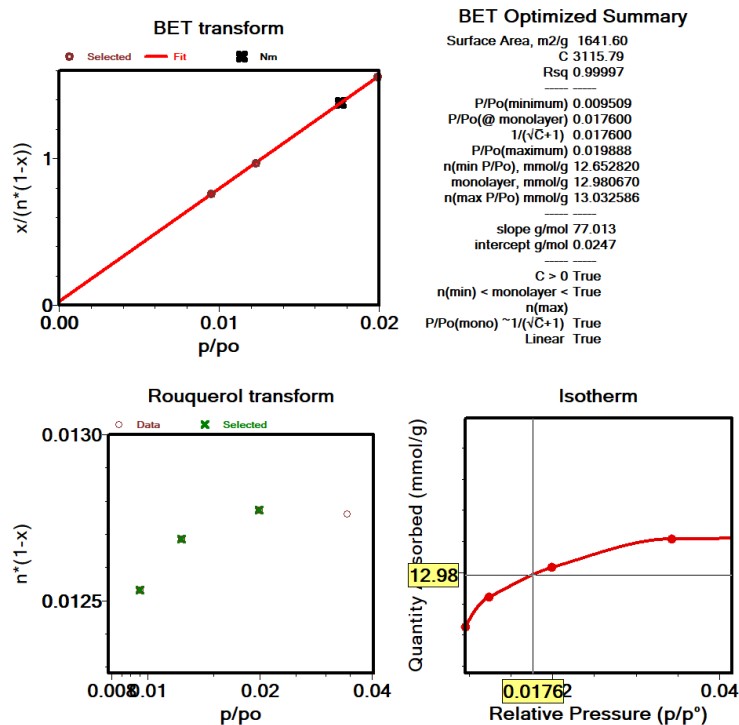


Figure S8. BET transform, Rouquerol transform and BET summary of UiO-66 for Kr isotherm at 77 K.

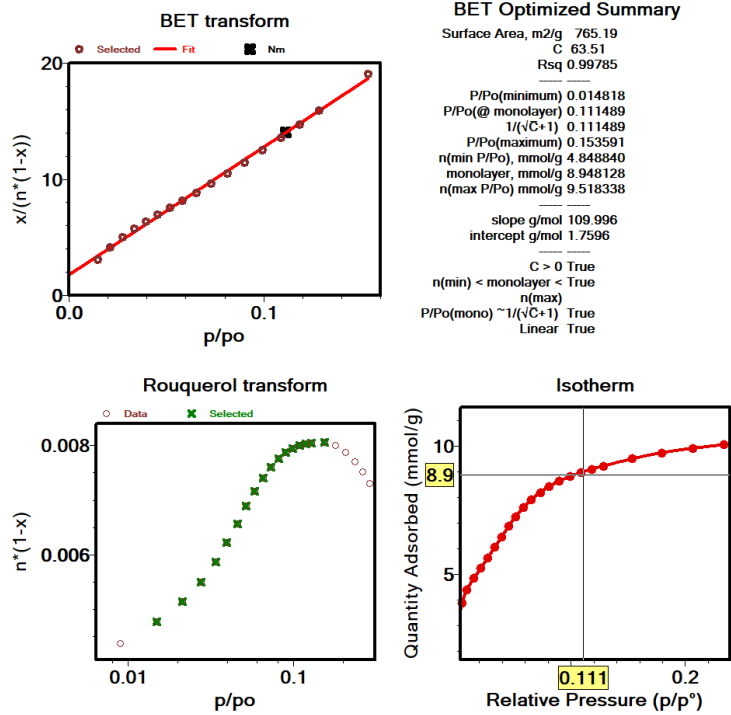


Figure S9. BET transform, Rouquerol transform and BET summary of UiO-66 for CO₂ isotherm at 195 K.

S2.3 SIFSIX-3-Ni

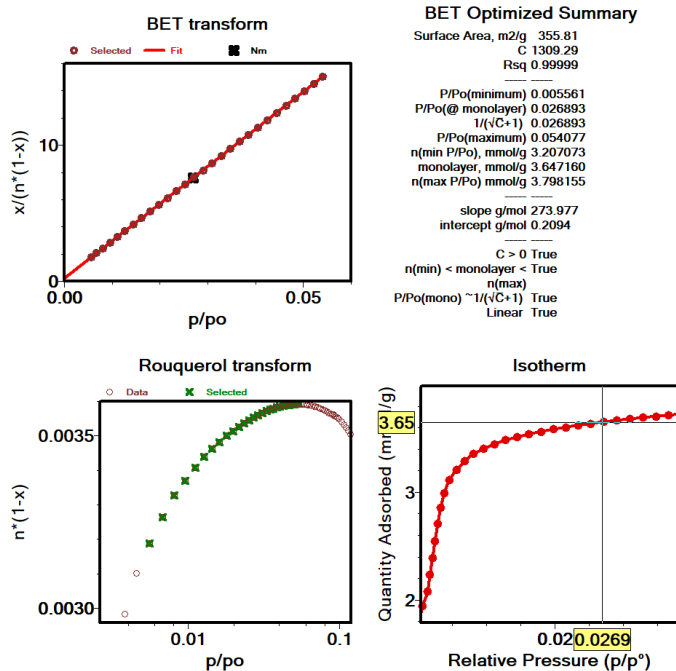


Figure S10. BET transform, Rouquerol transform and BET summary of SIFSIX-3-Ni for N₂ isotherm at 77 K.

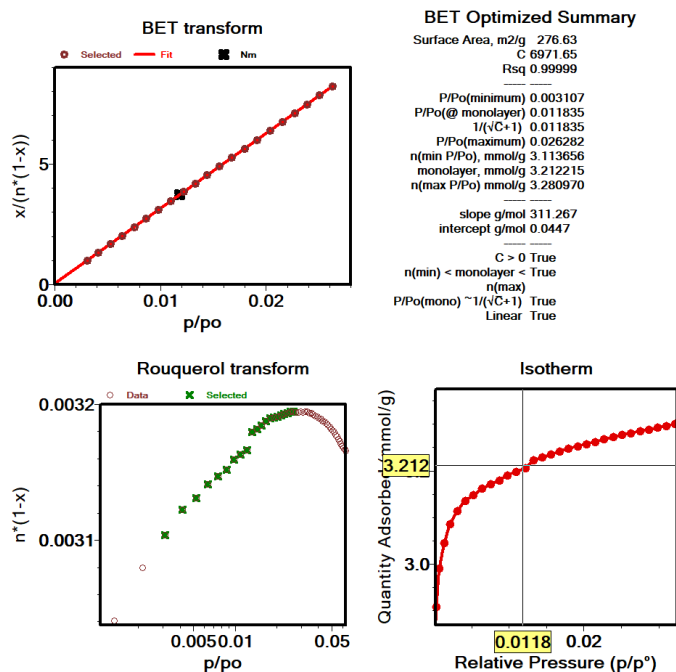


Figure S11. BET transform, Rouquerol transform and BET summary of SIFSIX-3-Ni for Ar isotherm at 87 K.

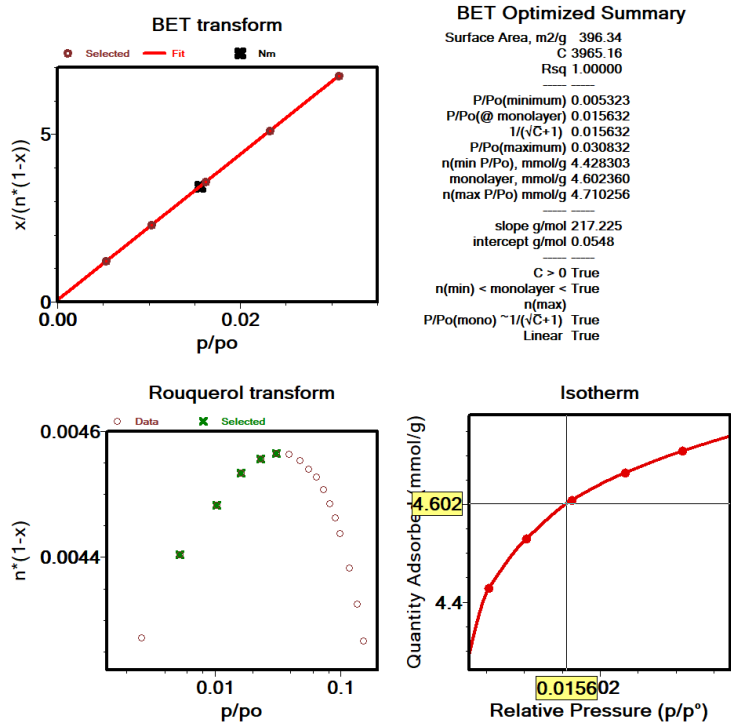


Figure S12. BET transform, Rouquerol transform and BET summary of SIFSIX-3-Ni for O₂ isotherm at 77 K.

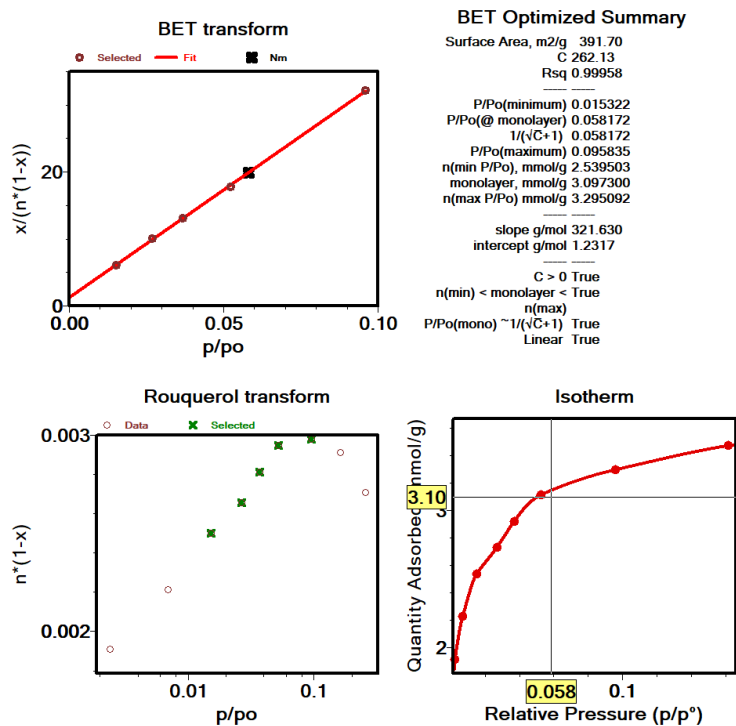


Figure S13. BET transform, Rouquerol transform and BET summary of SIFSIX-3-Ni for Kr isotherm at 77 K.

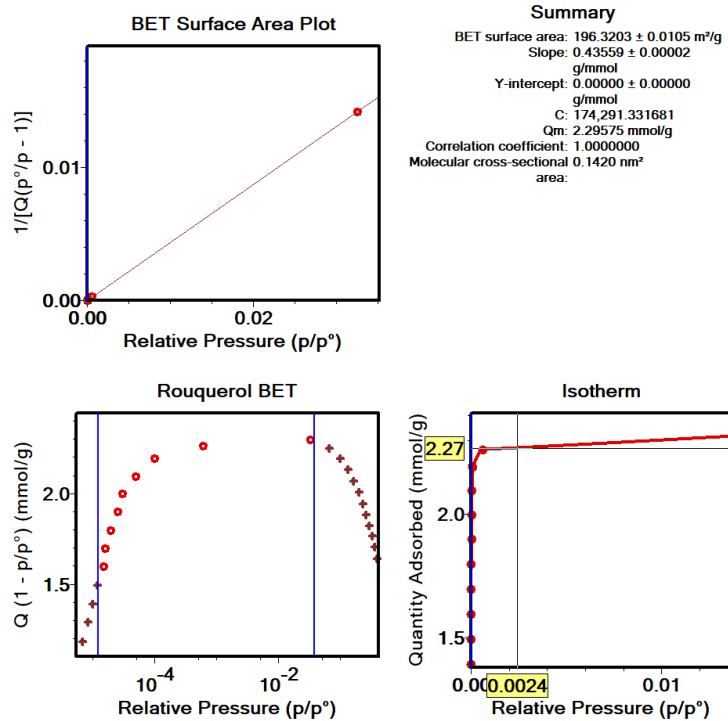


Figure S14. BET transform, Rouquerol transform and BET summary of SIFSIX-3-Ni for CO₂ isotherm at 195 K.

S2.4 NU-1000

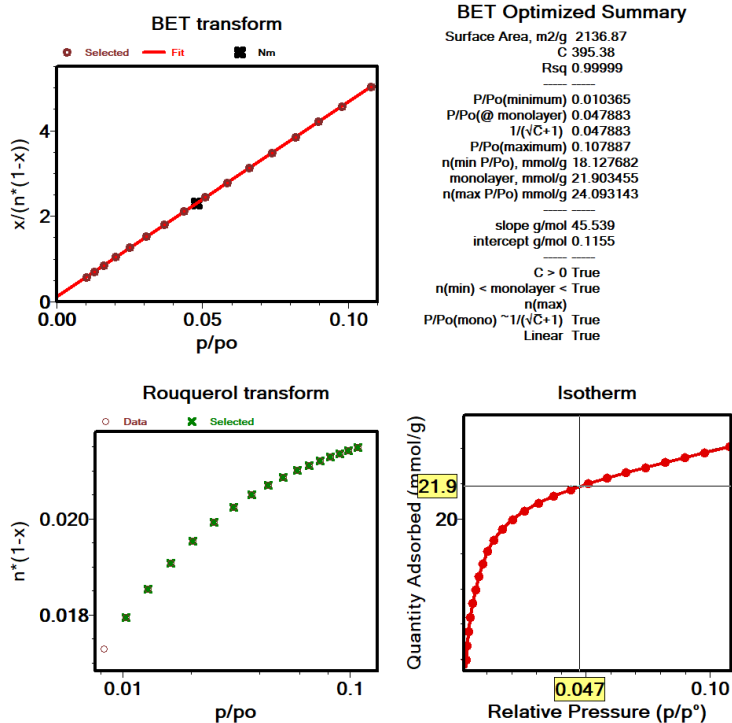


Figure S15. BET transform, Rouquerol transform and BET summary of NU-1000 for N₂ isotherm at 77 K.

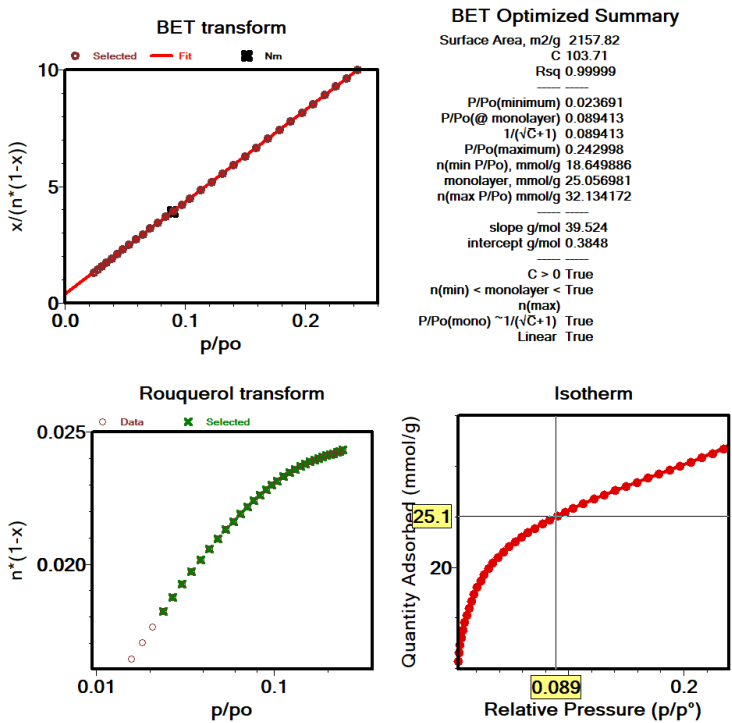


Figure S16. BET transform, Rouquerol transform and BET summary of NU-1000 for Ar isotherm at 87 K.

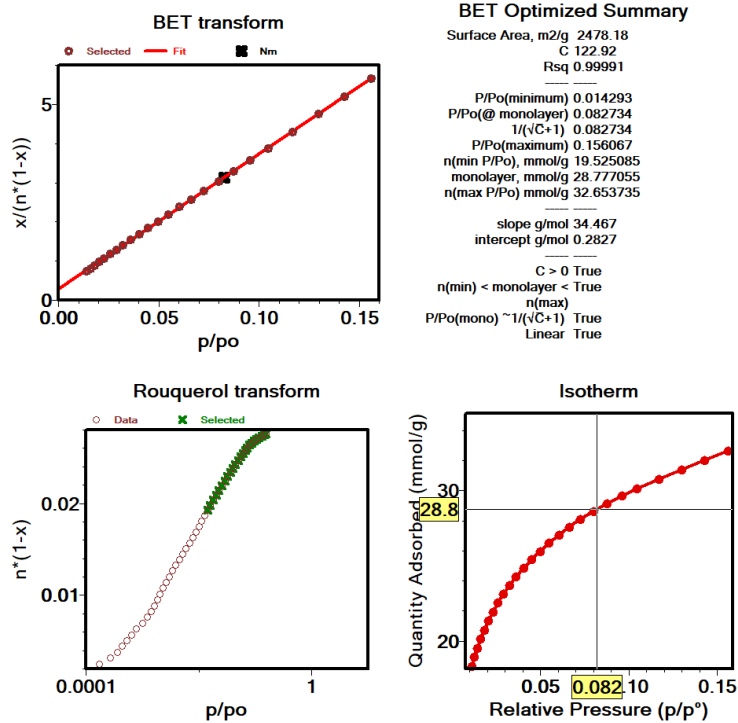


Figure S17. BET transform, Rouquerol transform and BET summary of NU-1000 for O₂ isotherm at 77 K.

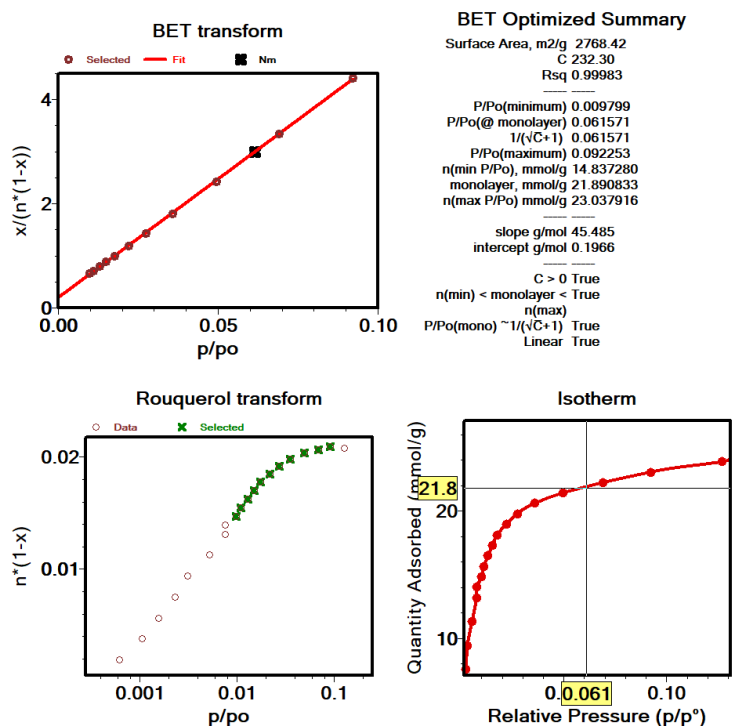


Figure S18. BET transform, Rouquerol transform and BET summary of NU-1000 for Kr isotherm at 77 K.

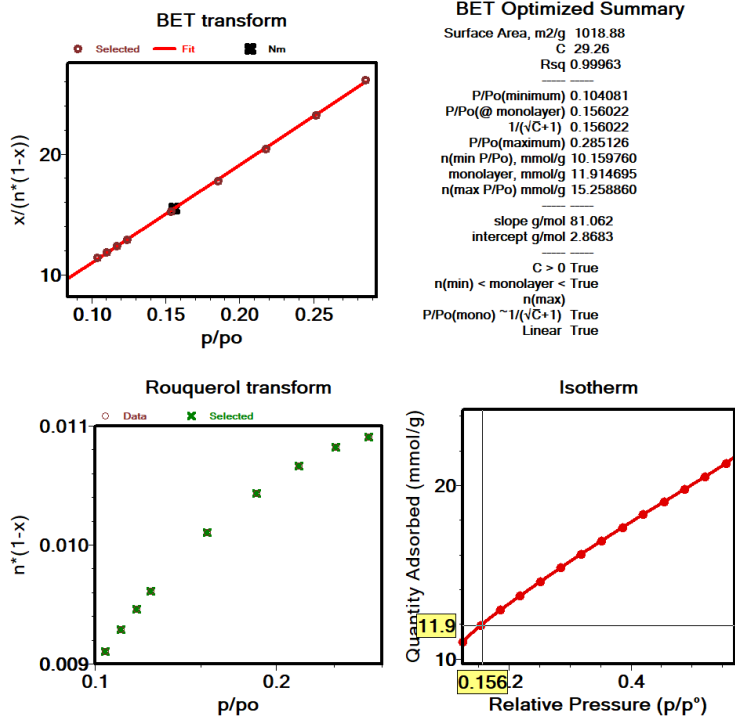


Figure S19. BET transform, Rouquerol transform and BET summary of NU-1000 for CO₂ isotherm at 195 K.

S2.5 ZIF-8

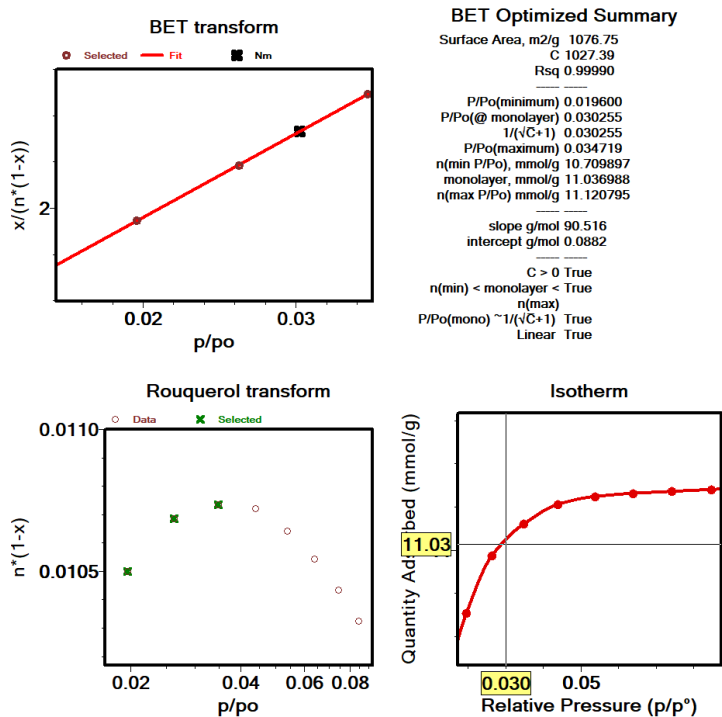


Figure S20. BET transform, Rouquerol transform and BET summary of ZIF-8 for N₂ isotherm at 77 K.

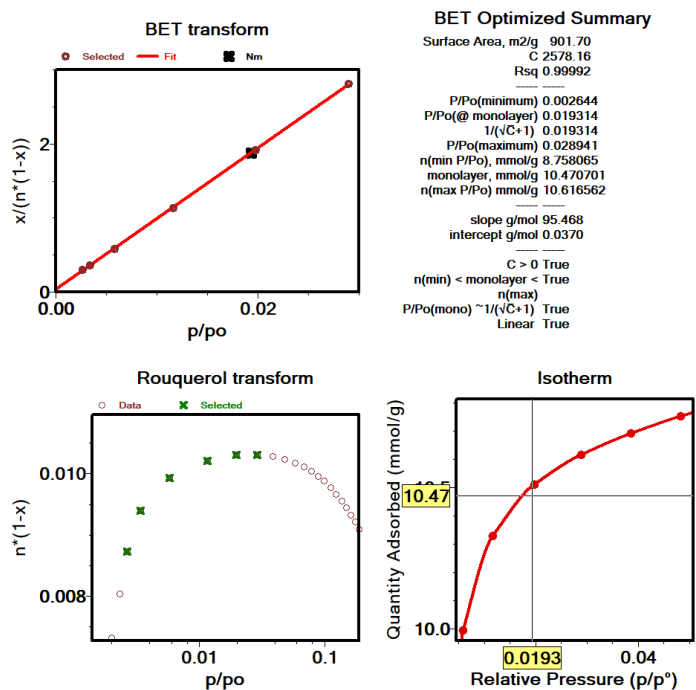


Figure S21. BET transform, Rouquerol transform and BET summary of ZIF-8 for Ar isotherm at 87 K.

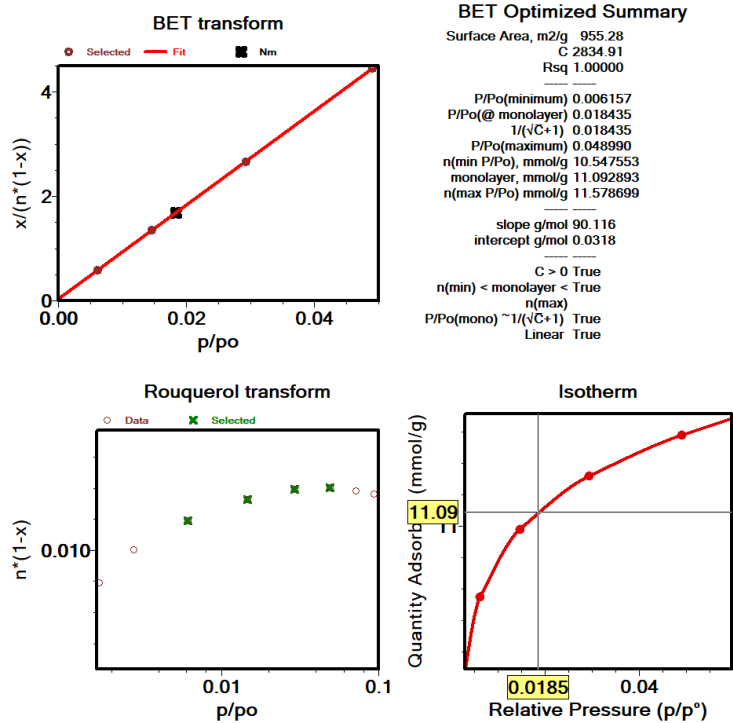


Figure S22. BET transform, Rouquerol transform and BET summary of ZIF-8 for O₂ isotherm at 77 K.

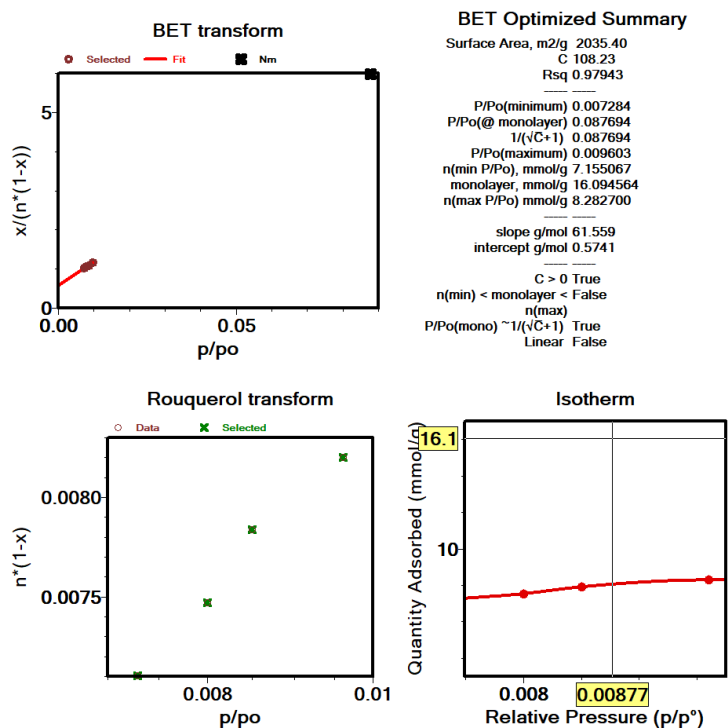


Figure S23. BET transform, Rouquerol transform and BET summary of ZIF-8 for Kr isotherm at 77 K.

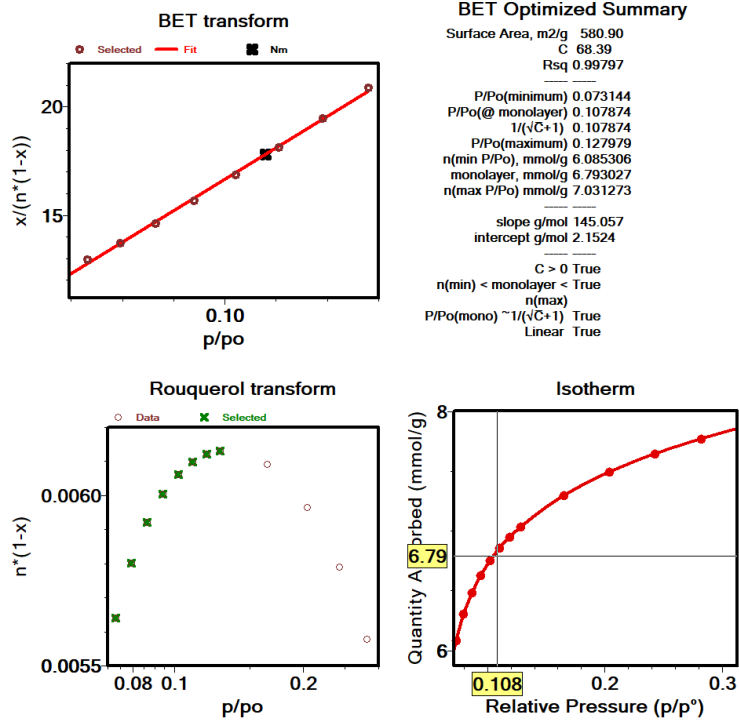


Figure S24. BET transform, Rouquerol transform and BET summary of ZIF-8 for CO₂ isotherm at 195 K.

S2.6 HKUST-1

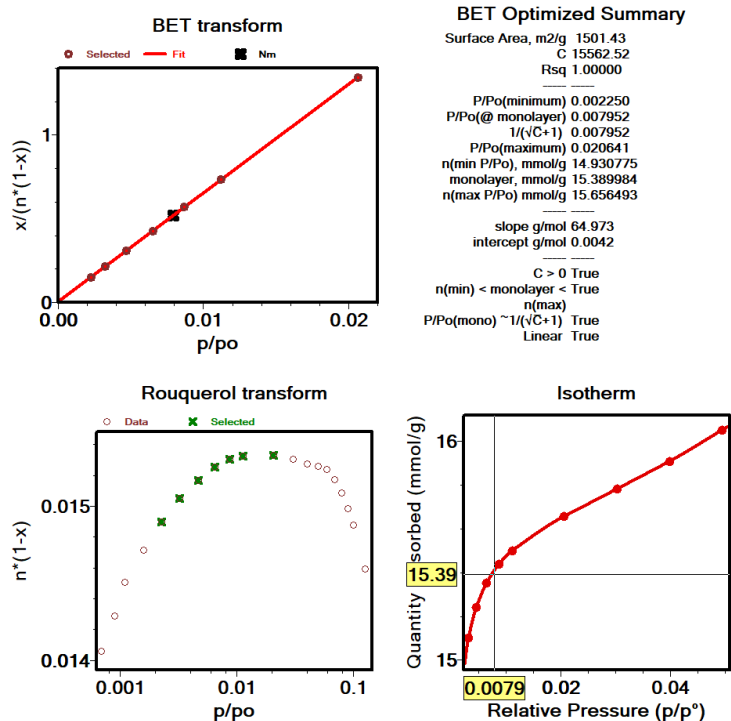


Figure S25. BET transform, Rouquerol transform and BET summary of HKUST-1 for N₂ isotherm at 77 K.

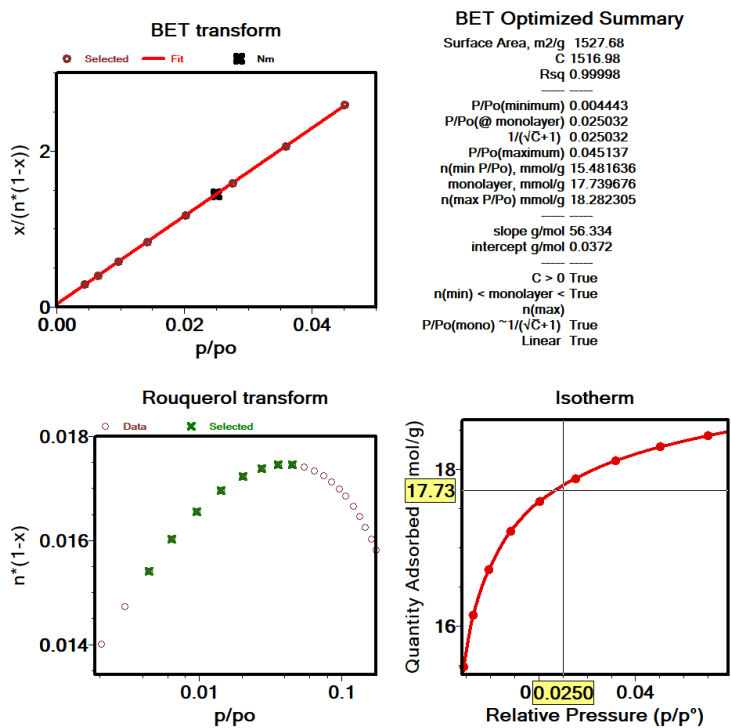


Figure S26. BET transform, Rouquerol transform and BET summary of HKUST-1 for Ar isotherm at 87 K.

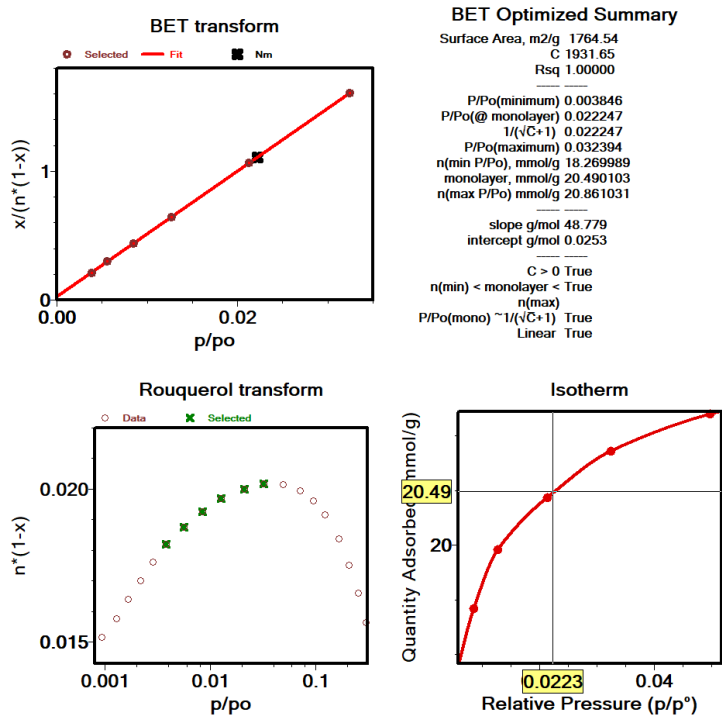


Figure S27. BET transform, Rouquerol transform and BET summary of HKUST-1 for O₂ isotherm at 77 K.

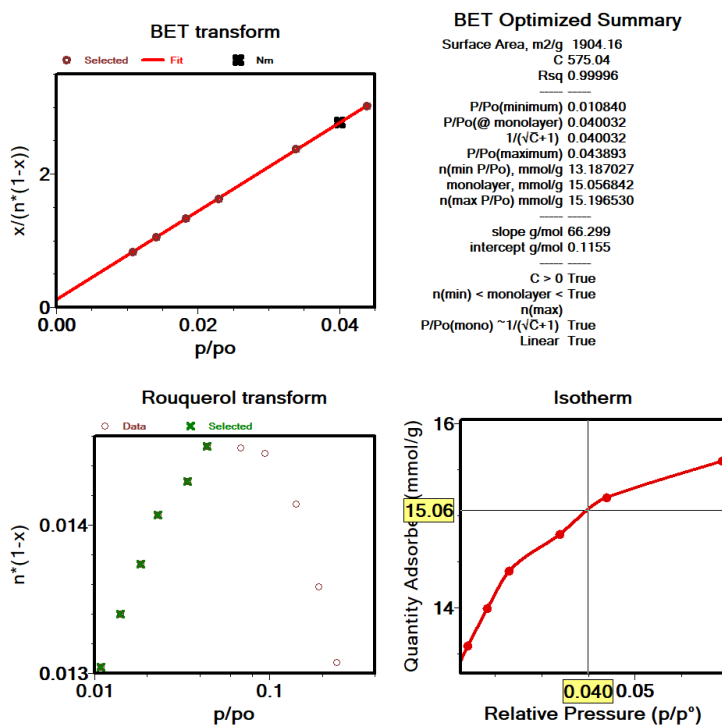


Figure S28. BET transform, Rouquerol transform and BET summary of HKUST-1 for Kr isotherm at 77 K.

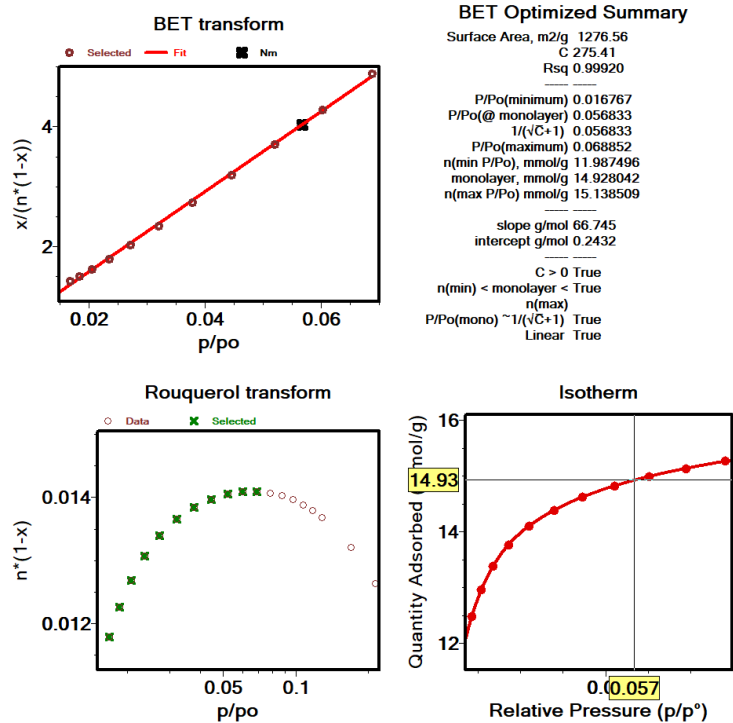


Figure S29. BET transform, Rouquerol transform and BET summary of HKUST-1 for CO₂ isotherm at 195 K.

S2.7 NU-1200

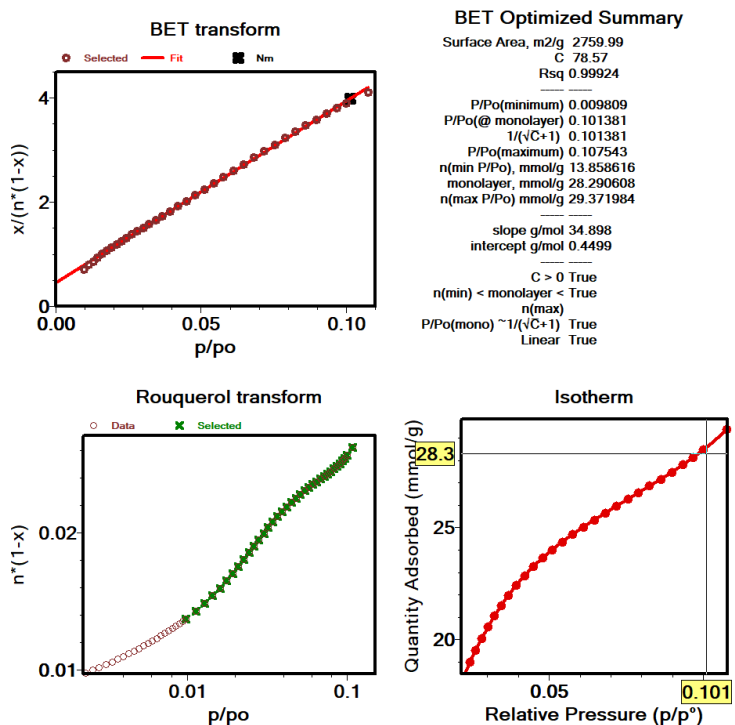


Figure S30. BET transform, Rouquerol transform and BET summary of NU-1200 for N₂ isotherm at 77 K.

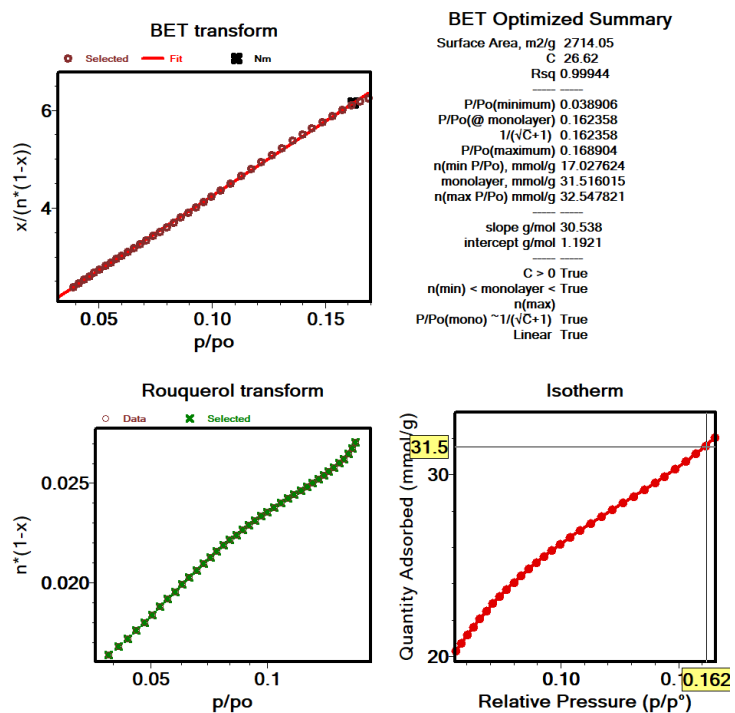


Figure S31. BET transform, Rouquerol transform and BET summary of NU-1200 for Ar isotherm at 87 K.

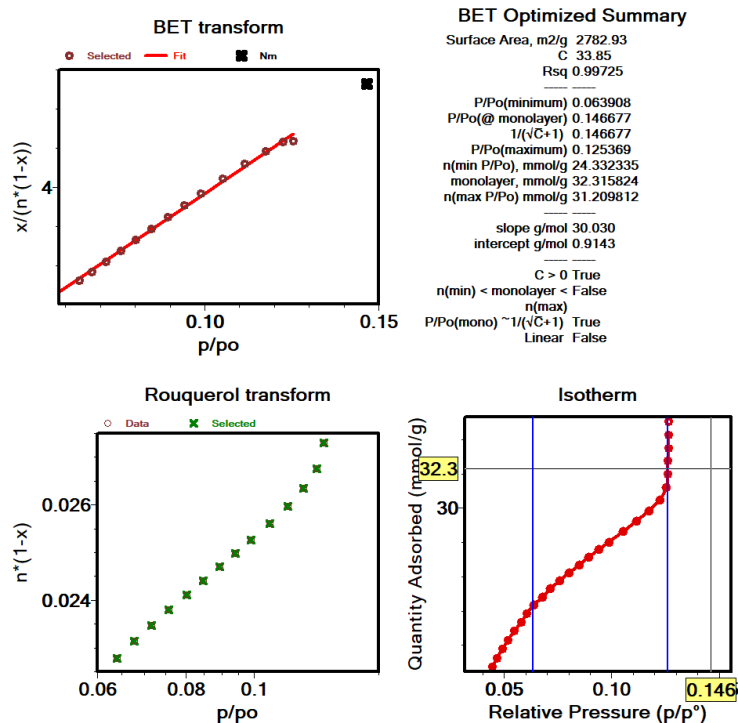


Figure S32. BET transform, Rouquerol transform and BET summary of NU-1200 for O₂ isotherm at 77 K.

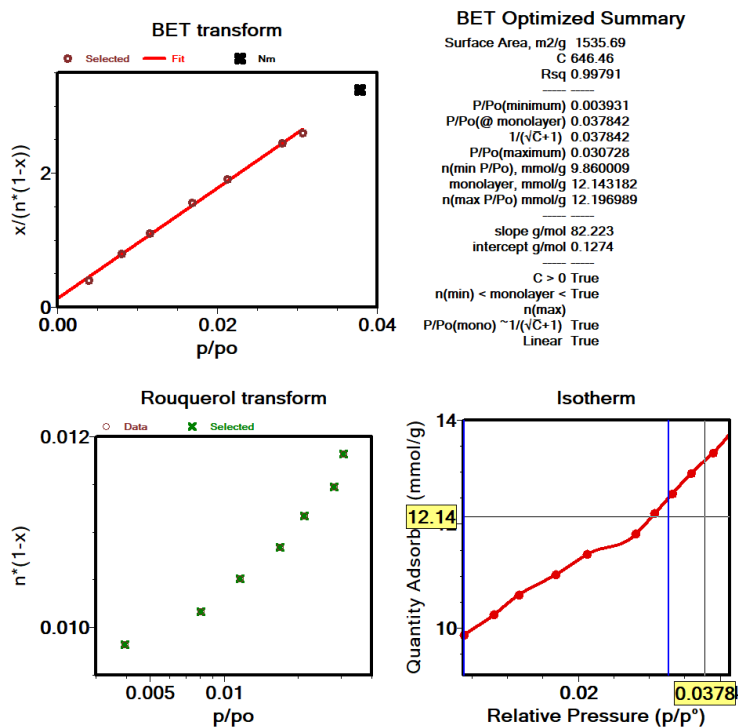


Figure S33. BET transform, Rouquerol transform and BET summary of NU-1200 for Kr isotherm at 77 K.

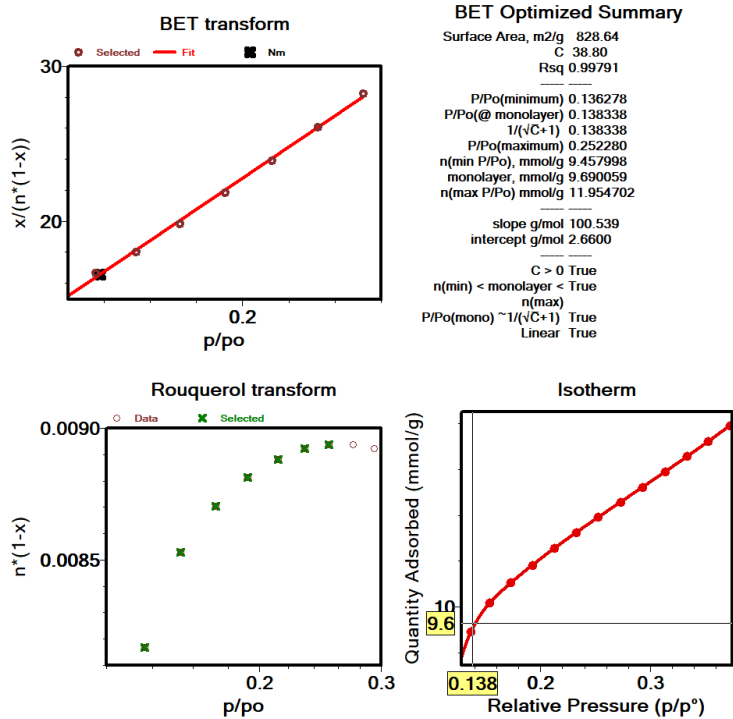


Figure S34. BET transform, Rouquerol transform and BET summary of NU-1200 for CO₂ isotherm at 195 K.

S2.8 Fe-NU-1500

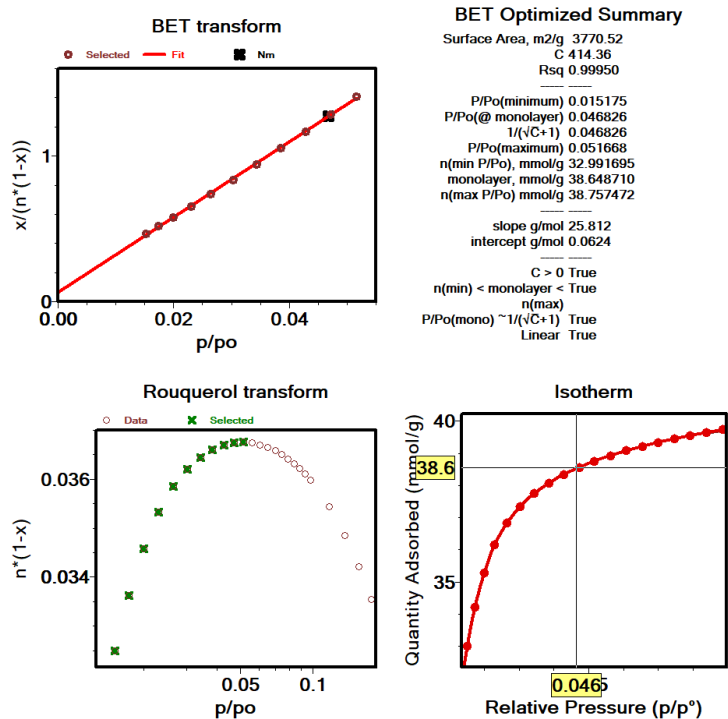


Figure S35. BET transform, Rouquerol transform and BET summary of Fe-NU-1500 for N₂ isotherm at 77 K.

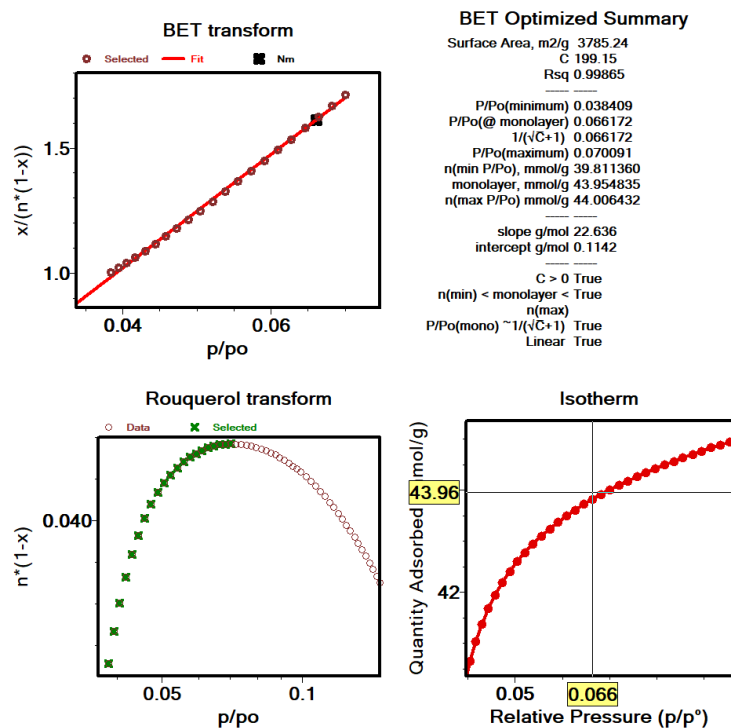


Figure S36. BET transform, Rouquerol transform and BET summary of Fe-NU-1500 for Ar isotherm at 87 K.

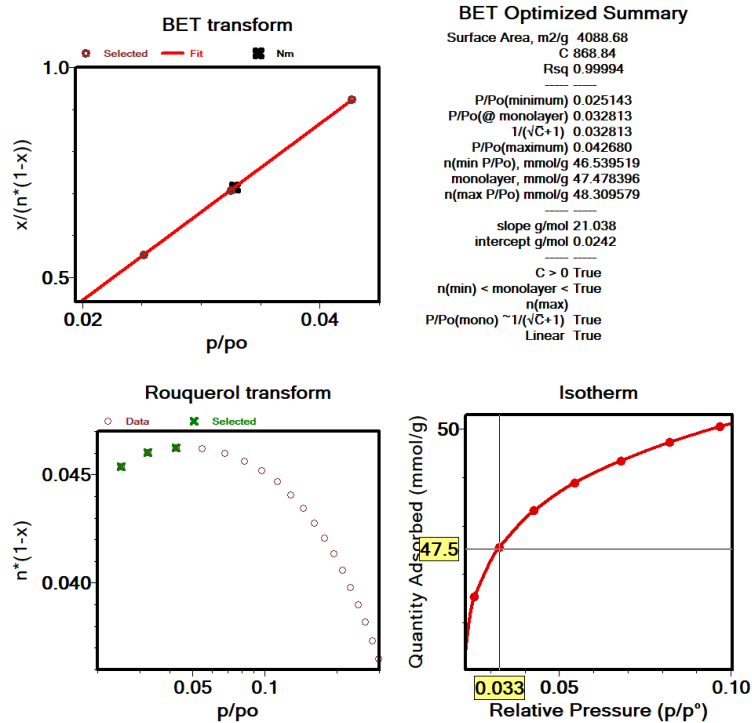


Figure S37. BET transform, Rouquerol transform and BET summary of Fe-NU-1500 for O₂ isotherm at 77 K.

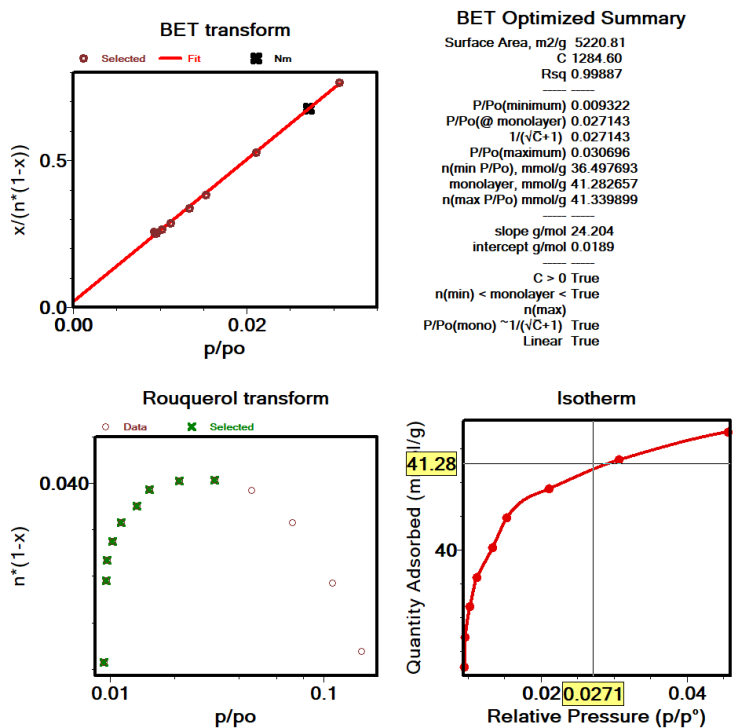


Figure S38. BET transform, Rouquerol transform and BET summary of Fe-NU-1500 for Kr isotherm at 77 K.

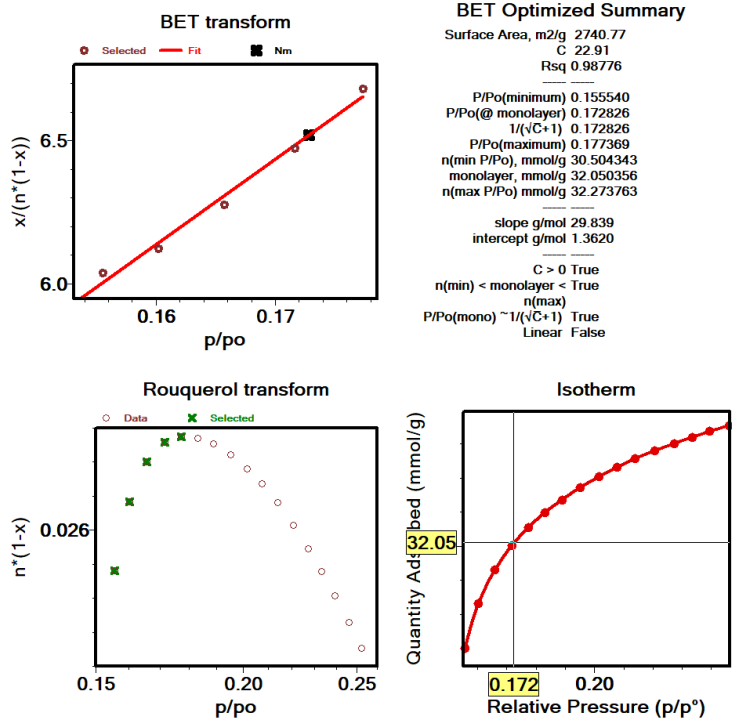


Figure S39. BET transform, Rouquerol transform and BET summary of Fe-NU-1500 for CO₂ isotherm at 195 K.

S2.9 Mg-MOF-74

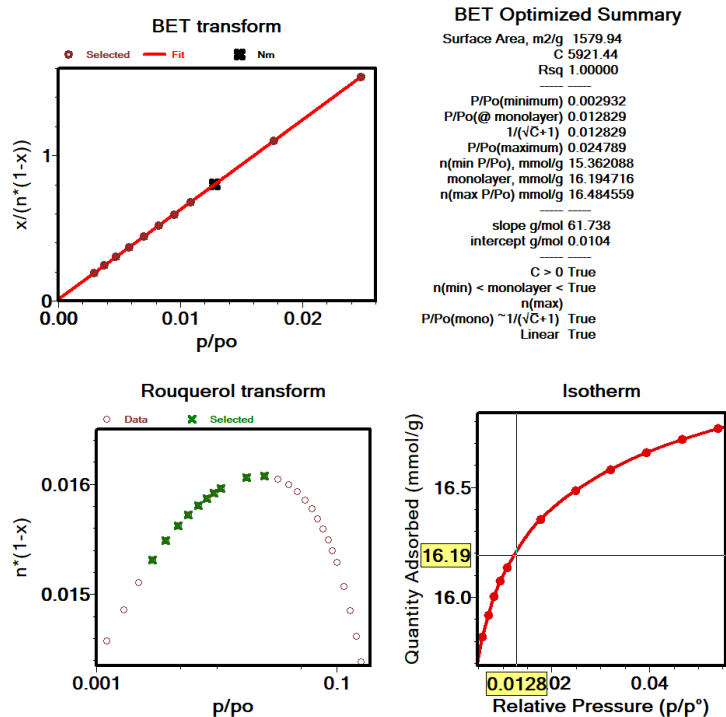


Figure S40. BET transform, Rouquerol transform and BET summary of Mg-MOF-74 for N₂ isotherm at 77 K.

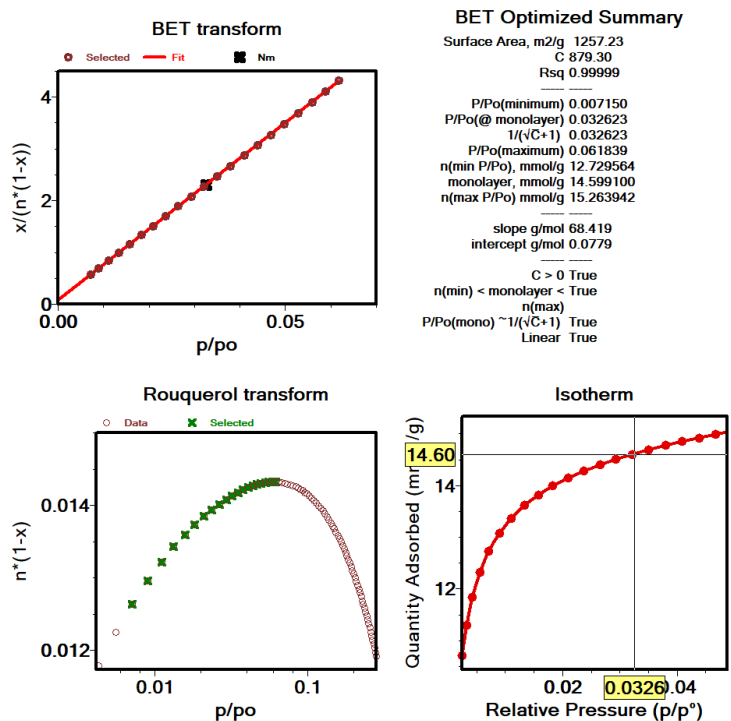


Figure S41. BET transform, Rouquerol transform and BET summary of Mg-MOF-74 for Ar isotherm at 87 K.

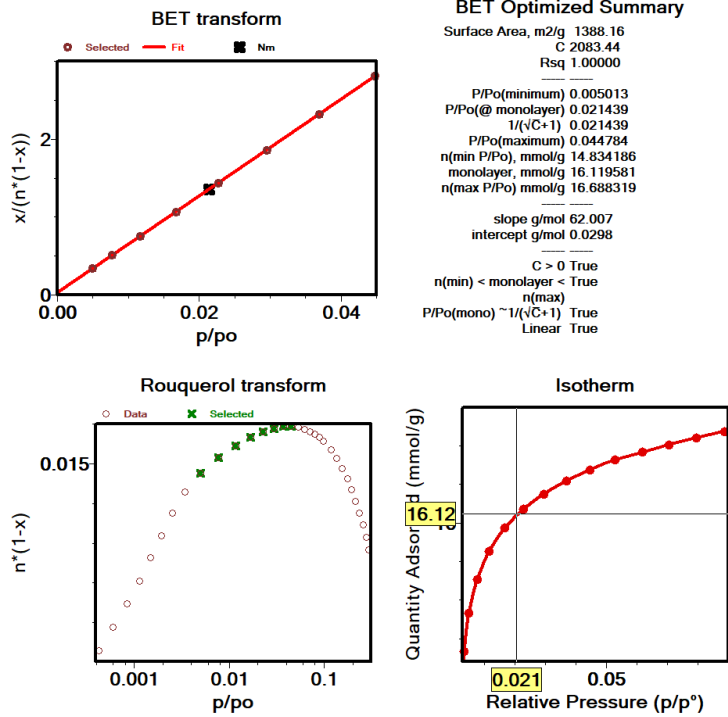


Figure S42. BET transform, Rouquerol transform and BET summary of Mg-MOF-74 for O₂ isotherm at 77 K.

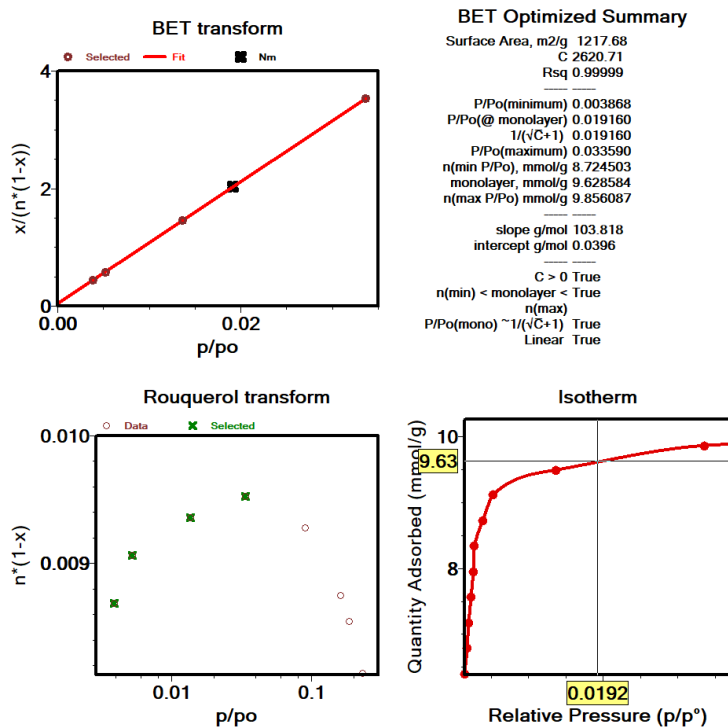


Figure S43. BET transform, Rouquerol transform and BET summary of Mg-MOF-74 for Kr isotherm at 77 K.

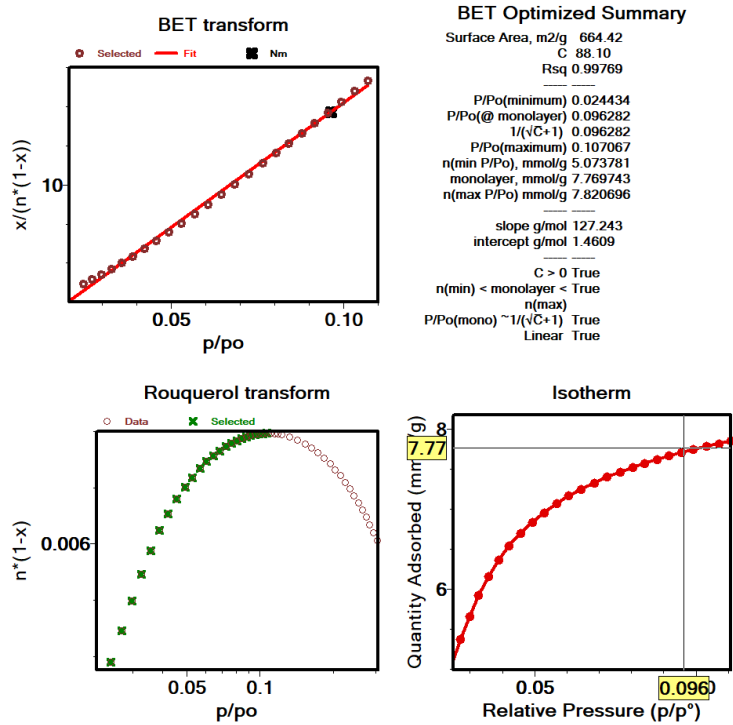


Figure S44. BET transform, Rouquerol transform and BET summary of Mg-MOF-74 for CO₂ isotherm at 195 K.

S2.10 MOF-808

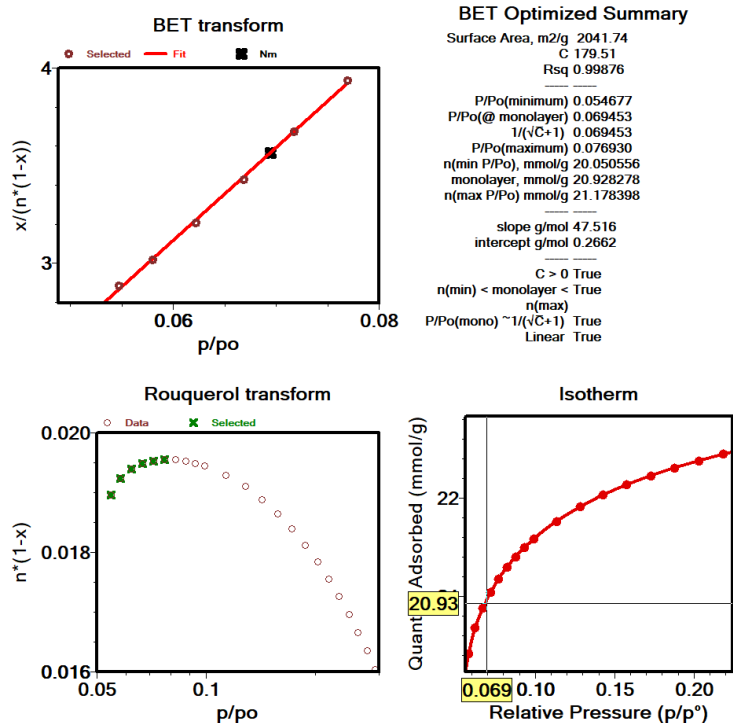


Figure S45. BET transform, Rouquerol transform and BET summary of MOF-808 for N₂ isotherm at 77 K.

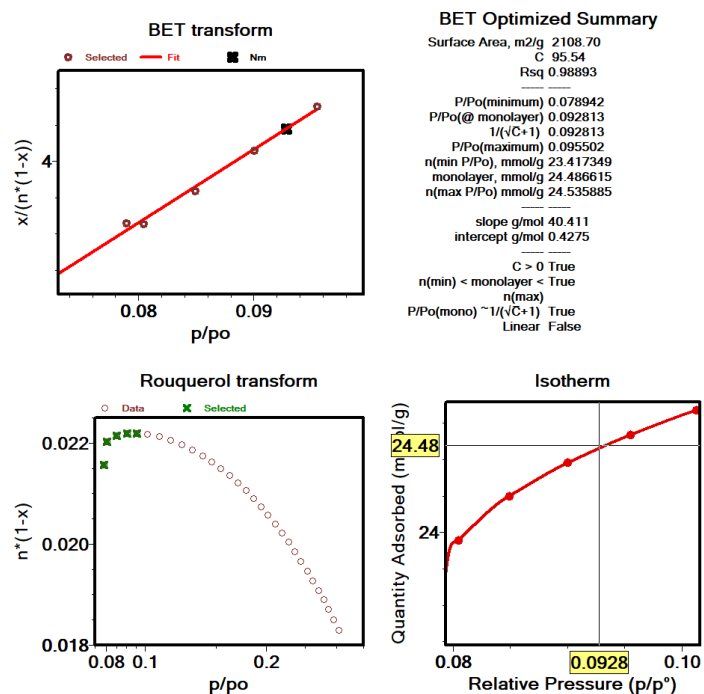


Figure S46. BET transform, Rouquerol transform and BET summary of MOF-808 for Ar isotherm at 87 K.

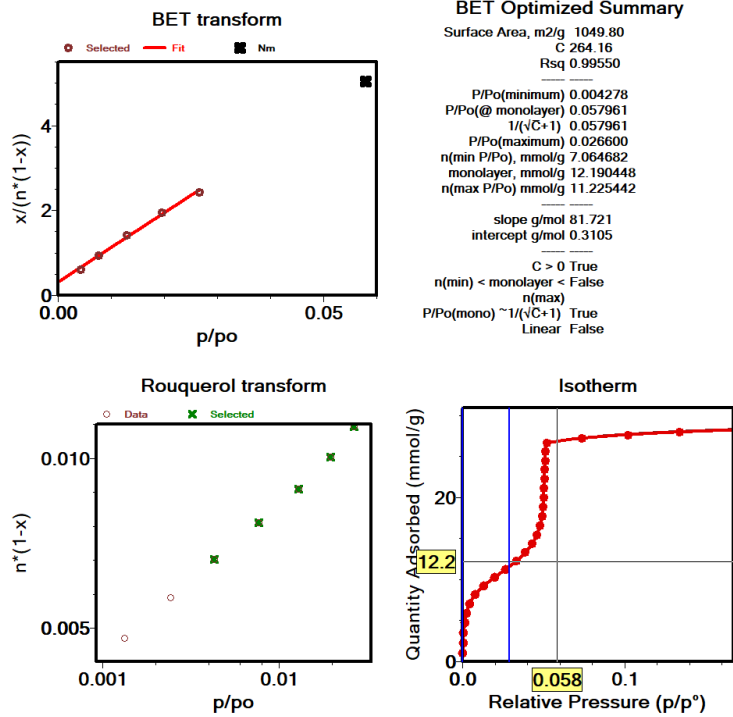


Figure S47. BET transform, Rouquerol transform and BET summary of MOF-808 for O₂ isotherm at 77 K.

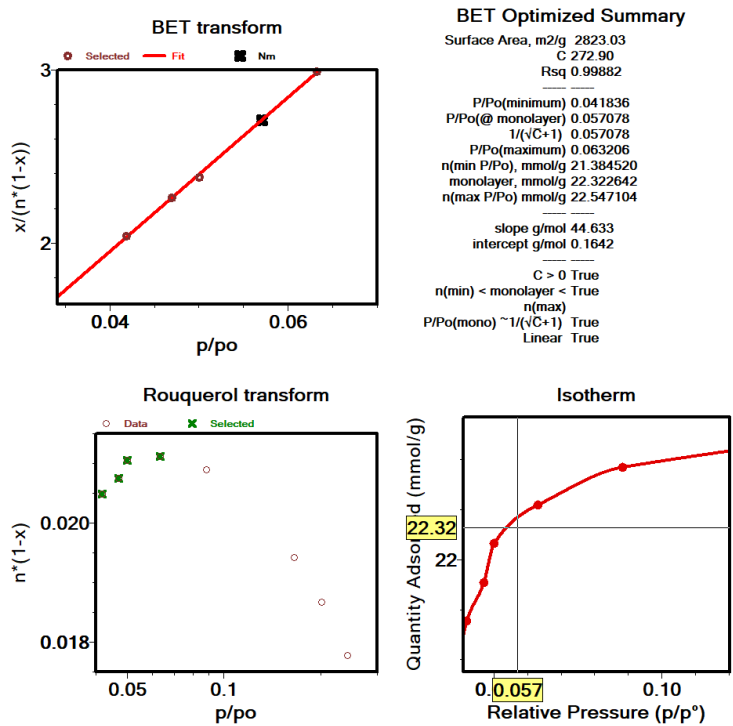


Figure S48. BET transform, Rouquerol transform and BET summary of MOF-808 for Kr isotherm at 77 K.

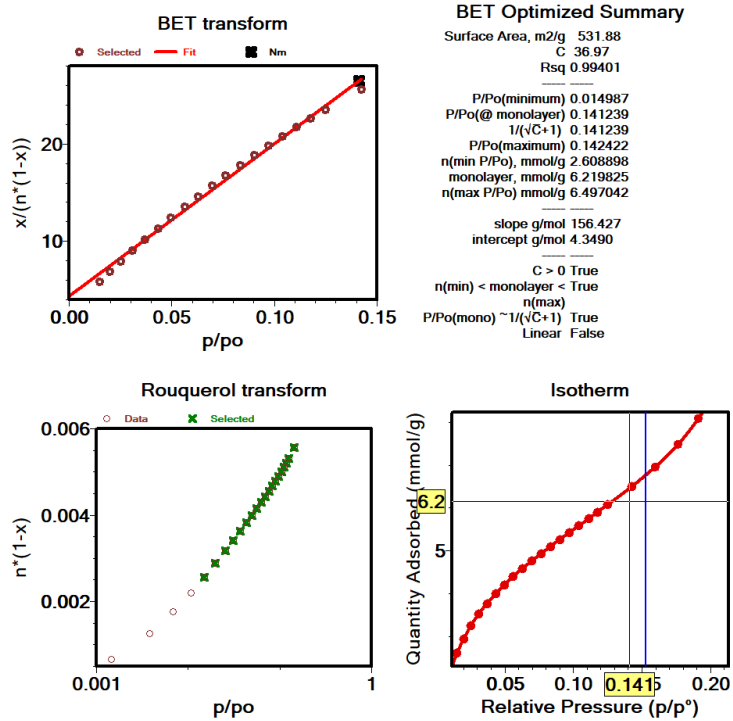


Figure S49. BET transform, Rouquerol transform and BET summary of MOF-808 for CO₂ isotherm at 195 K.

S3. Pore size distribution from CO₂ isotherms at 273 K

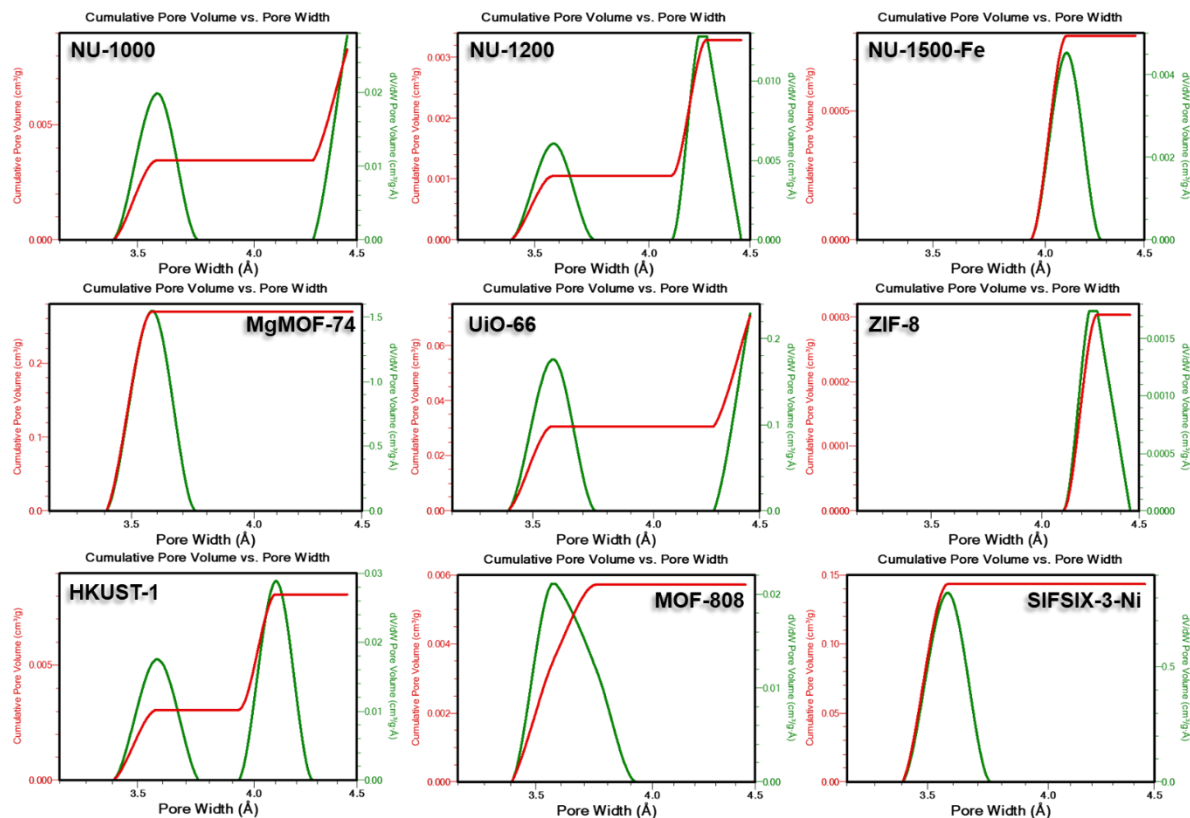


Figure S50. Pore size distribution analysis of NU-1000, NU-1200, NU-1500-Fe, MgMOF-74, UiO-66, ZIF-8, HKUST-1, MOF-808, and SIFSIX-3-Ni using NLDFT model for CO₂ 273K. While PSD plots of MOFs with expected ultramicropores such as SIFSIX-3-Ni show reasonable PSD profile, other MOFs that do not contain ultramicropores, also show similar PSD profiles. Therefore, one needs to be careful of analyzing the pore size distribution of MOFs with 273 K CO₂ isotherms. Extra care should be taken if the structure is unknown or the material is amorphous.

S4. ESW plots

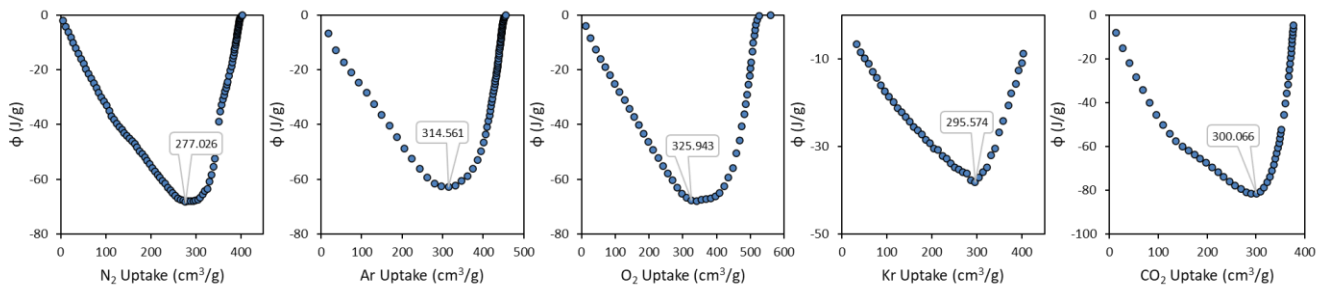


Figure S51. ESW plots for HKUST-1 using N₂ 77K, Ar 87K, Kr 77K, CO₂ 195K, and O₂ 77K.

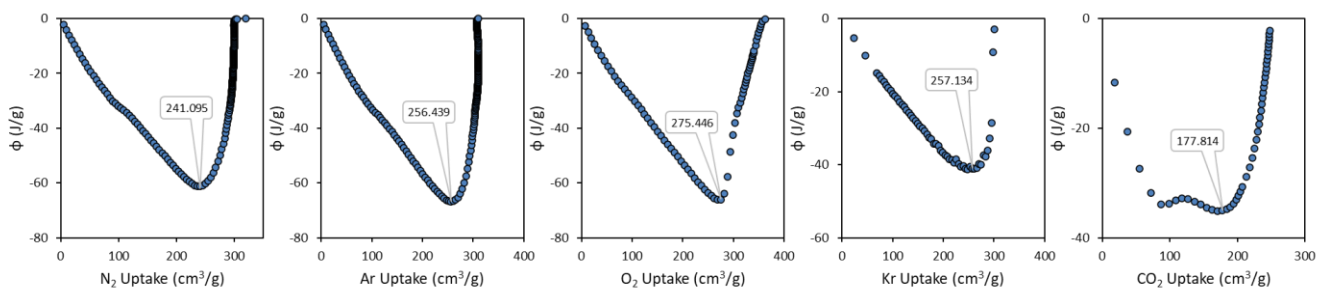


Figure S52. ESW plots for UiO-66 using N₂ 77K, Ar 87K, Kr 77K, CO₂ 195K, and O₂ 77K.

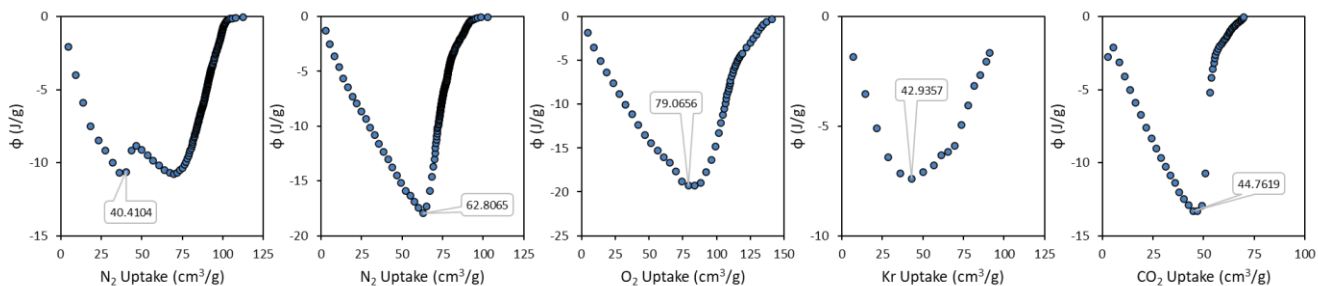


Figure S53. ESW plots for SIFSIX-3-Ni using N₂ 77K, Ar 87K, Kr 77K, CO₂ 195K, and O₂ 77K.

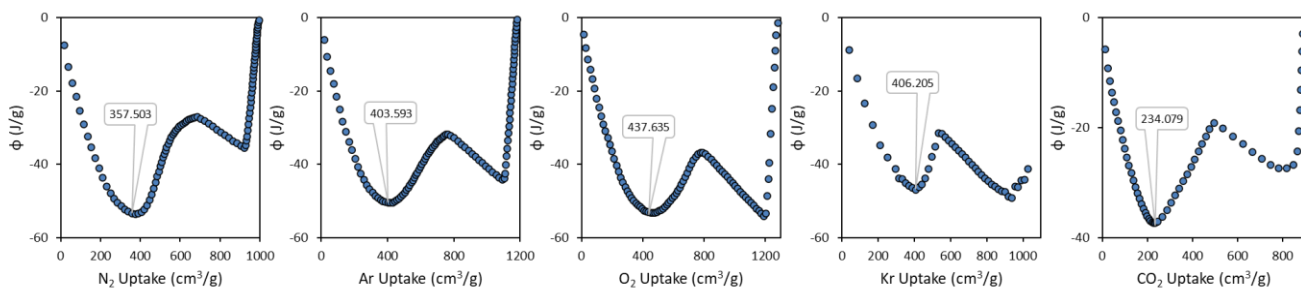


Figure S54. ESW plots for NU-1000 using N₂ 77K, Ar 87K, Kr 77K, CO₂ 195K, and O₂ 77K.

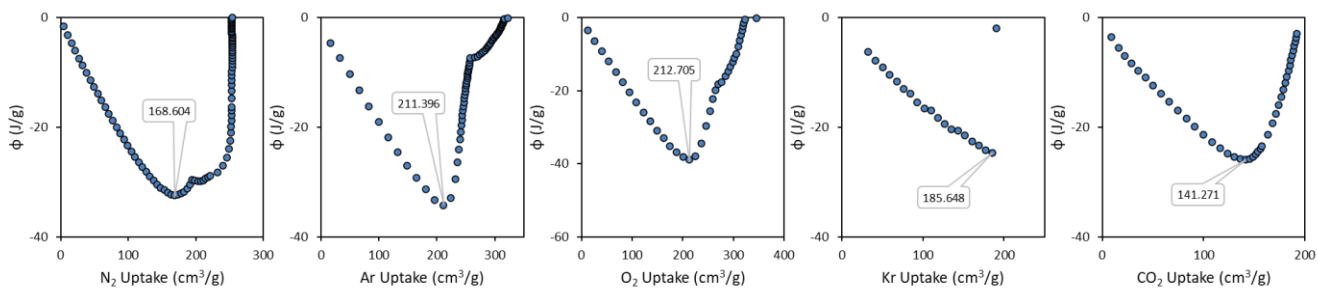


Figure S55. ESW plots for ZIF-8 using N₂ 77K, Ar 87K, Kr 77K, CO₂ 195K, and O₂ 77K.

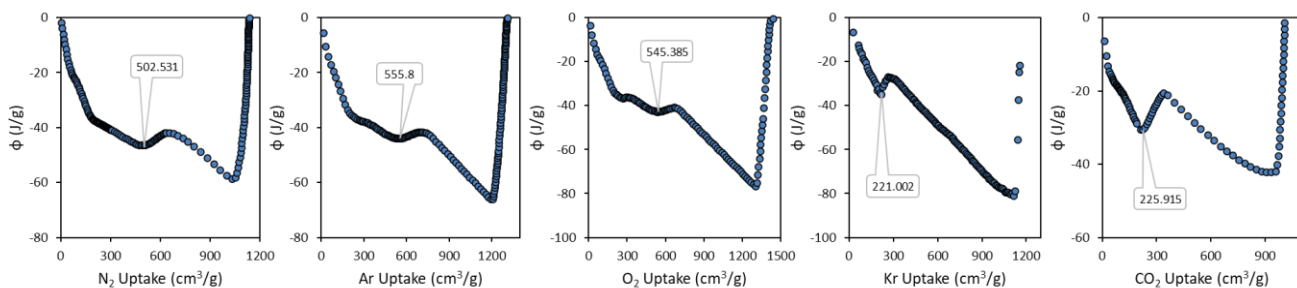


Figure S56. ESW plots for NU-1200 using N₂ 77K, Ar 87K, Kr 77K, CO₂ 195K, and O₂ 77K.

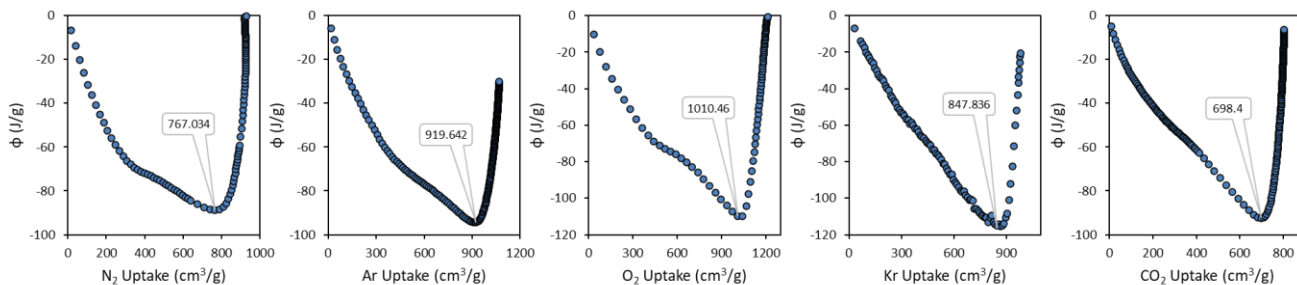


Figure S57. ESW plots for NU-1500-Fe using N₂ 77K, Ar 87K, Kr 77K, CO₂ 195K, and O₂ 77K.

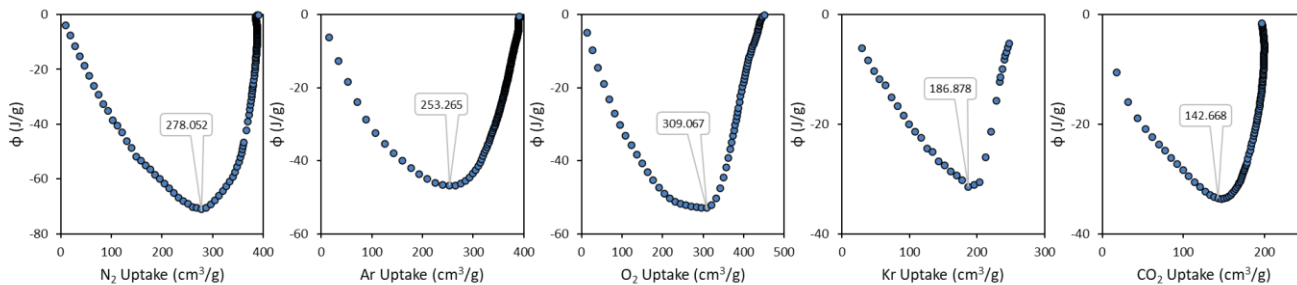


Figure S58. ESW plots for Mg-MOF-74 using N₂ 77K, Ar 87K, Kr 77K, CO₂ 195K, and O₂ 77K.

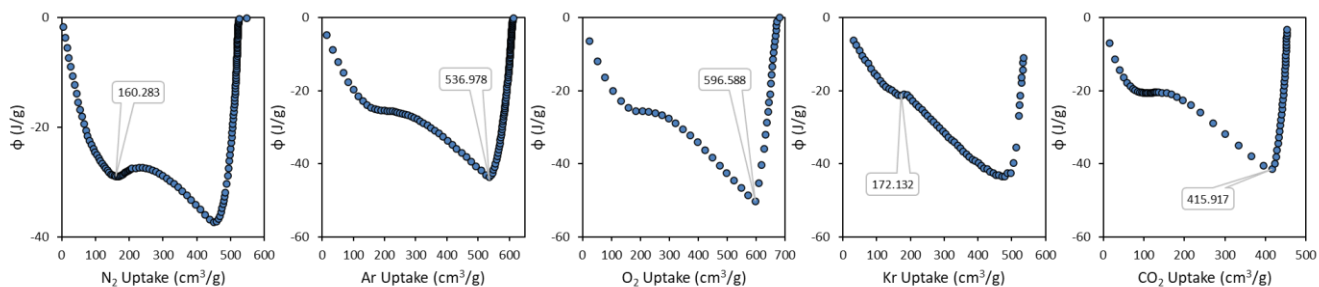


Figure S59. ESW plots for MOF-808 using N₂ 77K, Ar 87K, Kr 77K, CO₂ 195K, and O₂ 77K.

S4.1 BET+ESW tables

Table S5. BET+ESW area analysis for NU-1000, NU-1200, NU-1500-Fe, MgMOF-74, UiO-66, ZIF-8, HKUST-1, MOF-808, and SIFSIX-3-Ni using N₂ 77K, Ar 87K, Kr 77K, CO₂ 195K, and O₂ 77K.

UIO-66								
Isotherm	BET Surface Area (m ² /g)	Slope (g/cm ³ STP)	Y-intercept (g/cm ³ STP)	C	Q _m (cm ³ /g STP)	R ²	P/Po range	
N ₂ (77K)	1175	3.71E-03	< 1.0E-6	59881	270	0.99997	0.000092	0.000219
Ar (87K)	1115	3.45E-03	< 1.0E-6	23851	290	0.99998	0.000247	0.000558
Kr (77K)	1650	3.42E-03	2.00E-06	1999	292	0.99986	0.003700	0.009200
CO ₂ (195K)	860	4.31E-03	1.13E-04	39	226	0.99990	0.039200	0.073100
O ₂ (77K)	1130	3.40E-03	< 1.0E-6	56099	294	0.99997	0.000144	0.000910
SIFSIX-Ni								
Isotherm	BET Surface Area (m ² /g)	Slope (g/cm ³ STP)	Y-intercept (g/cm ³ STP)	C	Q _m (cm ³ /g STP)	R ²	P/Po range	
N ₂ (77K)	190	2.27E-02	< 1.0E-6	166580	44	0.99996	0.000003	0.000630
Ar (87K)	265	1.44E-02	< 1.0E-6	49959	69	0.99981	0.000100	0.000640
Kr (77K)	340	1.64E-02	1.50E-05	1089	61	0.99908	0.000400	0.030000
CO ₂ (195K)	195	1.94E+04	< 1.0E-6	175511	51	1.00000	0.000025	0.033000
O ₂ (77K)	375	1.03E-02	1.00E-06	19244	97	0.99995	0.000150	0.002600
NU-1000								
Isotherm	BET Surface Area (m ² /g)	Slope (g/cm ³ STP)	Y-intercept (g/cm ³ STP)	C	Q _m (cm ³ /g STP)	R ²	P/Po range	
N ₂ (77K)	2100	2.07E-03	4.00E-06	481	482	0.99999	0.008400	0.025200
Ar (87K)	2090	1.82E-03	1.50E-05	123	544	0.99998	0.023500	0.043200
Kr (77K)	2850	1.97E-03	1.00E-05	203	505	0.99990	0.012900	0.036000
CO ₂ (195K)	1035	3.55E-03	1.36E-04	27	271	0.99990	0.110000	0.218000
O ₂ (77K)	2150	1.78E-03	8.00E-06	232	560	0.99994	0.008900	0.016100
ZIF-8								
Isotherm	BET Surface Area (m ² /g)	Slope (g/cm ³ STP)	Y-intercept (g/cm ³ STP)	C	Q _m (cm ³ /g STP)	R ²	P/Po range	
N ₂ (77K)	875	4.98E-03	1.00E-06	4315	201	1.00000	0.000860	0.002290
Ar (87K)	900	4.26E-03	2.00E-06	2578	235	0.99996	0.002660	0.028900
Kr (77K)	1865	3.00E-03	2.40E-05	126	330	0.93444	0.005090	0.008520
CO ₂ (195K)	605	6.18E-03	1.21E-04	52	159	0.99898	0.073200	0.110400
O ₂ (77K)	950	4.04E-03	1.00E-06	3315	247	0.99999	0.001040	0.014600

Table S5 continues

HKUST-1								
Isotherm	BET Surface Area (m ² /g)	Slope (g/cm ³ STP)	Y-intercept (g/cm ³ STP)	C	Q _m (cm ³ /g STP)	R ²	P/Po range	
N ₂ (77K)	1460	2.98E+03	< 1.0E-6	22553	336	1.00000	0.000300	0.000900
Ar (87K)	1465	2.62E-03	1.90E-05	2324	381	0.99990	0.001100	0.006500
Kr (77K)	1905	2.96E-03	5.00E-06	575	337	0.99998	0.011000	0.044000
CO ₂ (195K)	1340	2.84E-03	1.40E-05	202	351	0.99961	0.018400	0.037700
O ₂ (77K)	1545	2.49E-03	< 1.0E-6	6054	402	0.99988	0.000470	0.001700
NU-1200								
Isotherm	BET Surface Area (m ² /g)	Slope (g/cm ³ STP)	Y-intercept (g/cm ³ STP)	C	Q _m (cm ³ /g STP)	R ²	P/Po range	
N ₂ (77K)	2770	1.55E-03	2.10E-05	76	637	0.99997	0.032300	0.044800
Ar (87K)	2690	1.38E-03	5.10E-05	28	699	0.99998	0.073800	0.089800
Kr (77K)	1500	3.77E-03	5.00E-06	813	265	0.99942	0.003960	0.028200
CO ₂ (195K)	845	4.39E-03	1.34E-04	34	221	0.99882	0.137000	0.234000
O ₂ (77K)	2765	1.35E-03	3.90E-05	35	720	0.99940	0.054900	0.071600
NU-1500-Fe								
Isotherm	BET Surface Area (m ² /g)	Slope (g/cm ³ STP)	Y-intercept (g/cm ³ STP)	C	Q _m (cm ³ /g STP)	R ²	P/Po range	
N ₂ (77K)	3970	1.09E-03	4.00E-06	268	912	0.99974	0.015100	0.030200
Ar (87K)	4050	9.41E-04	8.00E-06	118	1054	0.99978	0.041700	0.048900
Kr (77K)	5245	1.08E-03	1.00E-06	1412	930	0.99990	0.009600	0.021100
CO ₂ (195K)	2395	1.57E-03	2.00E-05	80	628	0.99842	0.160300	0.189000
O ₂ (77K)	4025	9.53E-04	1.00E-06	1182	1048	0.99981	0.022000	0.068000
MOF-74-Mg								
Isotherm	BET Surface Area (m ² /g)	Slope (g/cm ³ STP)	Y-intercept (g/cm ³ STP)	C	Q _m (cm ³ /g STP)	R ²	P/Po range	
N ₂ (77K)	1405	3.10E-03	< 1.0E-6	44566	322	0.99994	0.000110	0.000610
Ar (87K)	1215	3.17E-03	3.00E-06	1230	316	0.99995	0.002400	0.009000
Kr (77K)	1235	4.57E-03	2.00E-06	1855	219	0.99971	0.002350	0.013600
CO ₂ (195K)	700	5.40E-03	7.30E-05	75	183	0.99984	0.038700	0.056800
O ₂ (77K)	1370	2.80E-03	1.00E-06	2537	357	1.00000	0.001500	0.007700
MOF-808								
Isotherm	BET Surface Area (m ² /g)	Slope (g/cm ³ STP)	Y-intercept (g/cm ³ STP)	C	Q _m (cm ³ /g STP)	R ²	P/Po range	
N ₂ (77K)	860	5.05E-03	2.00E-06	2347	198	0.99993	0.001520	0.003460
Ar (87K)	1923	2.00E-03	2.00E-06	1173	500	0.99978	0.080300	0.108400
Kr (77K)	1275	4.41E-03	2.00E-05	224	226	0.99873	0.008300	0.020000
CO ₂ (195K)	2785	2.02E-03	8.00E-06	256	494	0.99820	0.034900	0.089000
O ₂ (77K)	1900	2.04E-03	-2.00E-05	-99	495	0.99892	0.053000	0.205000

Table S6. DFT kernels used for pore size distributions of N₂ (77K), Ar (87K), and O₂ (77K) isotherms.

MOF	N ₂ (77 K)	Ar (87 K)	O ₂ (77 K)
UiO-66	DFT > Cylinder > N2 Cylindrical Pores - Oxide Surface	DFT > Cylinder > HS-2D-NLDFT, Cylindrical Oxide, Ar, 87	DFT > Cylinder > O2 oxide cylinder
SIFSIX-3-Ni	DFT > Cylinder > NLDFT for Pillared Clay	DFT > Slit > Ar@87Carb Finite Pores, As=4, 2D-NLDFT	DFT > Cylinder > O2 oxide cylinder
NU-1000	DFT > Slit > N2-DFT Model	DFT > Cylinder > NLDFT-Argon on Oxide At 87 Kelvin	DFT > Cylinder > O2 oxide cylinder
ZIF-8	DFT > Cylinder > NLDFT for Pillared Clay	DFT > Cylinder > HS-2D-NLDFT, Cylindrical Oxide, Ar, 87	DFT > Cylinder > O2 oxide cylinder
HKUST-1	DFT > Cylinder > NLDFT for Pillared Clay	DFT > Cylinder > HS-2D-NLDFT, Cylindrical Oxide, Ar, 87	DFT > Cylinder > O2 oxide cylinder
NU-1200	DFT > Slit > N2-DFT Model	DFT > Slit > AR-DFT Model	DFT > Cylinder > O2 oxide cylinder
NU-1500-Fe	DFT > Slit > N2-DFT Model	DFT > Slit > AR-DFT Model	DFT > Cylinder > O2 oxide cylinder
MOF-74-Mg	DFT > Cylinder > N2 Cylindrical Pores - Oxide Surface	DFT > Cylinder > HS-2D-NLDFT, Cylindrical Oxide, Ar, 87	DFT > Cylinder > O2 oxide cylinder
MOF-808	DFT > Cylinder > N2 Cylindrical Pores - Oxide Surface	DFT > Cylinder > HS-2D-NLDFT, Cylindrical Oxide, Ar, 87	DFT > Cylinder > O2 oxide cylinder ⁶

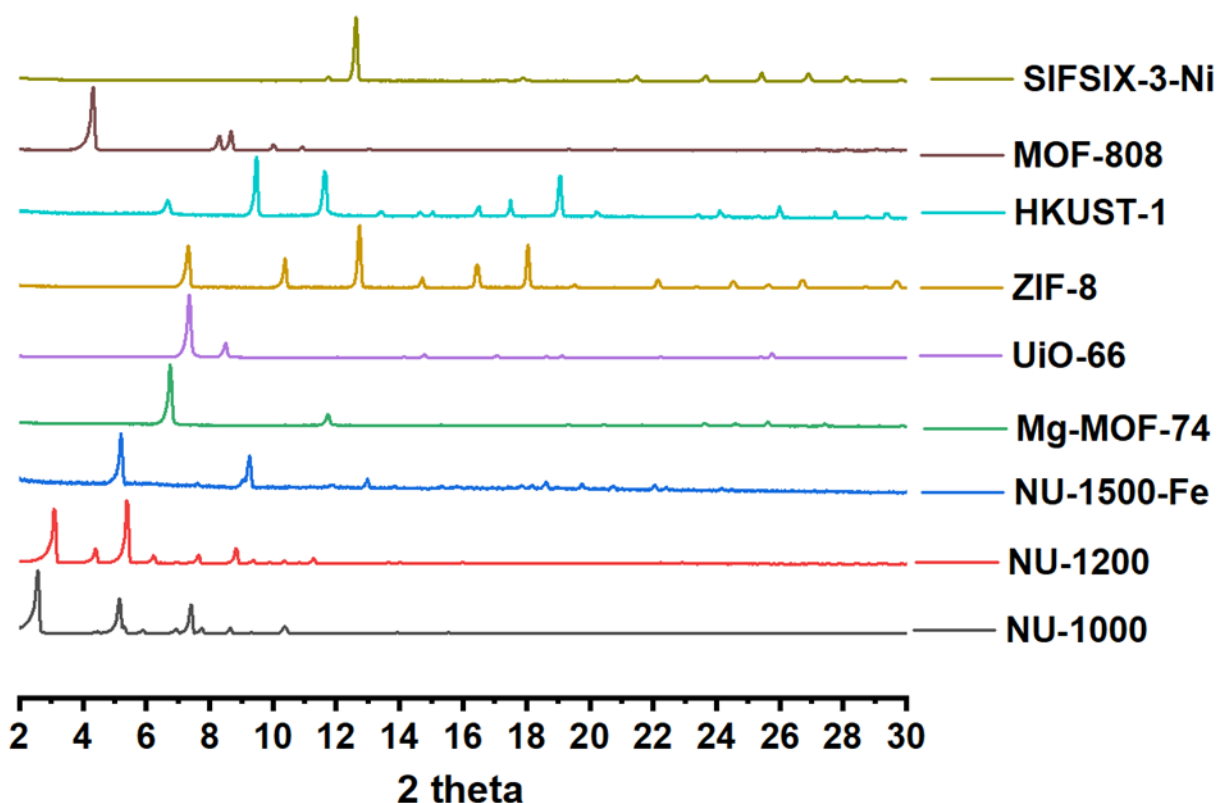


Figure S60. PXRD patterns of the MOFs studied here.

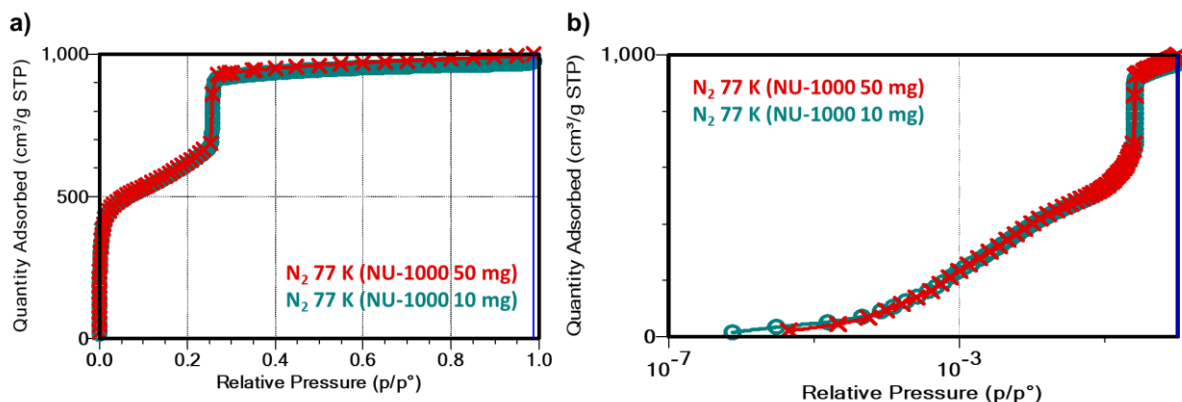


Figure S61. N_2 (77 K) isotherms of NU-1000 for 50 mg sample (red) and 10 mg sample (green) in (a) linear scale and (b) semi-logarithmic scale. We measured the nitrogen isotherm of a representative MOF, NU-1000, with low quantity (10 mg) to see the limit of N_2 with high surface area materials. N_2 isotherm of NU-1000 with only 10 mg and 50 mg powder material in the analysis tube was collected. It is clear that the isotherms are nearly identical, highlighting the applicability of N_2 isotherms at 77 K for the analysis of high surface area MOF materials with as low as 10 mg. *It is important to note that we do not recommend this as a standard practice, but rather for cases where larger quantities cannot be obtained such as radioactive materials, thin films etc.* This is because of the challenge in measuring the weight of activated sample accurately when dealing with low quantities. The percentage of error in weighing the sample will be directly

reflected on the adsorbed quantity, since the uptakes are normalized with the weight of the adsorbent. Therefore, we still recommend using 60–100 mg of the activated MOF material for collecting isotherm to minimize error propagation. If a facility with Kr isotherm capability is accessible, we still recommend to researchers who are working on materials with very low surface areas or materials where only few milligram quantities to follow the guidelines of IUPAC to obtain Kr isotherms for determining the BET areas.

References

1. Islamoglu, T.; Otake, K.-i.; Li, P.; Buru, C. T.; Peters, A. W.; Akpınar, I.; Garibay, S. J.; Farha, O. K. Revisiting the structural homogeneity of NU-1000, a Zr-based metal–organic framework. *CrystEngComm* **2018**, *20* (39), 5913-5918.
2. Chen, Z.; Li, P.; Zhang, X.; Li, P.; Wasson, M. C.; Islamoglu, T.; Stoddart, J. F.; Farha, O. K. Reticular Access to Highly Porous aCS-MOFs with Rigid Trigonal Prismatic Linkers for Water Sorption. *J. Am. Chem. Soc.* **2019**, *141* (7), 2900-2905.
3. Liu, T.-F.; Vermeulen, N. A.; Howarth, A. J.; Li, P.; Sarjeant, A. A.; Hupp, J. T.; Farha, O. K. Adding to the Arsenal of Zirconium-Based Metal–Organic Frameworks: the Topology as a Platform for Solvent-Assisted Metal Incorporation. *Eur. J. Inorg. Chem.* **2016**, *2016* (27), 4349-4352.
4. Grant Glover, T.; Peterson, G. W.; Schindler, B. J.; Britt, D.; Yaghi, O. MOF-74 building unit has a direct impact on toxic gas adsorption. *Chem. Eng. Sci.* **2011**, *66* (2), 163-170.
5. Idrees, K. B.; Chen, Z.; Zhang, X.; Mian, M. R.; Drout, R. J.; Islamoglu, T.; Farha, O. K. Tailoring Pore Aperture and Structural Defects in Zirconium-Based Metal–Organic Frameworks for Krypton/Xenon Separation. *Chem. Mater.* **2020**, *32* (9), 3776-3782.
6. Karagiari, O.; Lalonde, M. B.; Bury, W.; Sarjeant, A. A.; Farha, O. K.; Hupp, J. T. Opening ZIF-8: A Catalytically Active Zeolitic Imidazolate Framework of Sodalite Topology with Unsubstituted Linkers. *J. Am. Chem. Soc.* **2012**, *134* (45), 18790-18796.
7. Babaei, H.; DeCoster, M. E.; Jeong, M.; Hassan, Z. M.; Islamoglu, T.; Baumgart, H.; McGaughey, A. J. H.; Redel, E.; Farha, O. K.; Hopkins, P. E.; Malen, J. A.; Wilmer, C. E. Observation of reduced thermal conductivity in a metal-organic framework due to the presence of adsorbates. *Nat Commun* **2020**, *11* (1), 4010.
8. Islamoglu, T.; Ray, D.; Li, P.; Majewski, M. B.; Akpınar, I.; Zhang, X.; Cramer, C. J.; Gagliardi, L.; Farha, O. K. From Transition Metals to Lanthanides to Actinides: Metal-Mediated Tuning of Electronic Properties of Isostructural Metal–Organic Frameworks. *Inorg. Chem.* **2018**, *57* (21), 13246-13251.
9. Yancy-Caballero, D.; Leperi, K. T.; Bucior, B. J.; Richardson, R. K.; Islamoglu, T.; Farha, O. K.; You, F.; Snurr, R. Q. Process-level modelling and optimization to evaluate metal–organic frameworks for post-combustion capture of CO₂. *Mol Syst Des Eng* **2020**, *5* (7), 1205-1218.
10. Willems, T. F.; Rycroft, C. H.; Kazi, M.; Meza, J. C.; Haranczyk, M. Algorithms and tools for high-throughput geometry-based analysis of crystalline porous materials. *Microporous Mesoporous Mater.* **2012**, *149* (1), 134-141.